ELSEVIER

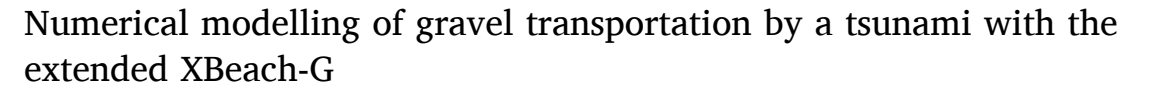
Contents lists available at ScienceDirect

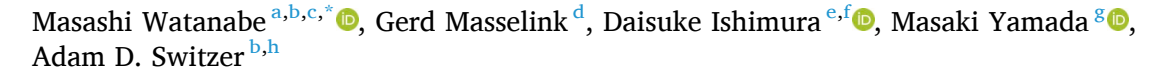
# Applied Ocean Research

journal homepage: www.elsevier.com/locate/apor



# Research paper





- <sup>a</sup> School of Ocean and Earth Science, University of Southampton, European Way, Southampton, SO14 3ZH, UK
- <sup>b</sup> Earth Observatory of Singapore, Nanyang Technological University, N2-01A-15, 50 Nanyang Avenue, 639798, Singapore
- <sup>c</sup> Research and Development Initiative, Chuo University, 1-13-27 Kasuga, Bunkyo-ku, Tokyo 112-8551, Japan
- d School of Marine Science and Engineering, Faculty of Science and Technology, Plymouth University, Drake Circus, Plymouth, Devon PL4 8AA, UK
- <sup>e</sup> Department of Geography, Tokyo Metropolitan University, 1-1 Minami-Osawa, Hachioji City, Tokyo 192-0397, Japan
- f Department of Earth Sciences, Chiba University, 1-33 Yayoi-cho, Inage-ku, Chiba 263-8522, Japan
- g Department of Geology, Faculty of Science, Shinshu University, 3-1-1 Asahi, Matsumoto, Nagano 390-8621, Japan
- <sup>h</sup> Asian School of the Environment, Nanyang Technological University, 50 Nanyang Drive, 639798, Singapore

#### ARTICLE INFO

#### Keywords: Gravel sediment transport Tsunami XBeach-G Numerical simulation

#### ABSTRACT

Estimating coastal erosion by a tsunami is essential for land use planning, assessing hazards for current structures (e.g., coastal nuclear power plants), and for paleotsunami reconstruction. Such estimations are currently available only for sandy beaches, using sand sediment transport models, which are not applicable to gravel beaches, which are the most common beach type in high-latitude settings. This study extended the one-dimensional crossshore XBeach-G model to account for two-dimensional gravel transport by a tsunami. First, this study confirmed that the extended XBeach-G model can simulate a time series of waveforms of solitary waves during laboratory experiments. The proposed model was then applied to gravel transport by the 2011 Tohoku-oki tsunami at Koyadori, Japan, and found that the simulation results were consistent with observations of gravel deposits in previous studies. It was revealed that infiltration and exfiltration have an impact on morphological change caused by a tsunami on gravel coasts. In the simulation, inundation depth over land by the tsunami increased due to groundwater exfiltration, which increased the onshore deposition volume of gravel tsunami deposits. The groundwater flow calculation has not been incorporated so far for tsunami modelling, but this is important for modelling tsunami inundation at gravel beaches and gravel sediment transport by a tsunami. However, choosing appropriate values for the sediment friction factor and multiplier in the equation for gravel transport is more critical to reproducing the deposition of gravel sediments by a tsunami because these parameters are more sensitive than the parameter of groundwater flow. Although the presented model has been developed for tsunami simulation on any gravel beach, further testing and validation are recommended.

# 1. Introduction

To investigate multiple recognised effects of tsunami impacts in coastal areas (e.g., the collapse of coastal protection facilities due to coastal erosion/sedimentation, port dysfunction due to change in coastline morphology and/or port depth, blockage of coastal power plant intakes by sand sediment), tsunami-driven sediment transport needs to be predicted. The transport of sand (grain size: 1/16 - 2 mm) by a tsunami has been modelled in many studies (e.g., Simpson and Castelltort, 2006; Gelfenbaum et al., 2007; Xiao et al., 2010; Apotsos et al.,

2011a, 2011b; Li et al., 2012; Sugawara et al., 2014). A sand sediment transport model is also a valid tool for investigating the size of paleotsunamis. Indeed, the reconstruction of paleotsunami has been conducted by investigating the size of paleotsunami that can explain the distribution of sandy deposits formed by paleotsunami using a sand sediment transport model (e.g., Sugawara et al., 2019).

However, such sediment transport models do not apply to gravel beaches, which are the most common beach type at high latitudes (Simpson, 2005). To date, numerical simulations which have been conducted to estimate the sizes of paleotsunamis that can explain data

E-mail address: masashi.watanabe@soton.ac.uk (M. Watanabe).

https://doi.org/10.1016/j.apor.2025.104765

<sup>\*</sup> Corresponding author.

collected during field surveys have considered mud sediment transport (grain size <1/16 mm) (e.g., Watanabe et al., 2023a) and boulder transport (grain size >256 mm) (e.g., Imamura et al., 2008; Watanabe et al., 2023b). However, the numerical model which can estimate the dynamics of gravel particles (grain size: 2 - 256 mm) during tsunamis has yet to be proposed, even though gravel layers formed by tsunamis have been amply reported (e.g., Moore, 2000; Nichol et al., 2003; Szczuciński et al., 2012; Yamada et al., 2014; Ishimura and Miyauchi, 2015; Inoue et al., 2017). To reconstruct paleotsunami from gravel tsunami deposits or investigate coastal erosion and sedimentation at gravel coasts, a numerical simulation model is needed to predict gravel transport by a tsunami.

The challenging part of predicting gravel sediment transport by a tsunami is that the transport mechanics differ from those of sand sediments. Sand sediments are transported as bedload or suspended load by a tsunami (e.g., Shinozaki et al., 2020). In contrast, gravel sediment is larger and heavier than sand sediment, so that gravel sediment transport has been assumed to be only bedload when simulating gravel sediment transport by water currents and waves (e.g., McCall et al., 2014). The other challenging part is that it has been revealed that groundwater flow on a gravel beach plays a significant role in determining the transport of gravel sediment by storm waves (e.g., Jamal et al., 2014); however, the effect of this process in the case of a tsunami remains unclear. This hydraulic process might need to be included when modelling gravel sediment transport by a tsunami.

A one-dimensional numerical simulation model has been proposed to predict gravel sediment transport by storm surge and waves, utilising XBeach (Jamal et al., 2014) or the XBeach-G model (McCall et al., 2014, 2015). The wave-resolving hydrodynamic module of XBeach has been demonstrated to accurately simulate wave transformation in both two-dimensional and one-dimensional settings (e.g., McCall et al., 2014; Quataert et al., 2020; De Beer et al., 2021; De Ridder et al., 2021). The XBeach model has been shown to accurately quantify storm impact, overwash and breaching processes on sandy beaches (Roelvink et al., 2009). XBeach-G is the model that is developed to model one-dimensional phase-resolving gravel sediment transport and morphological change by (storm) waves over gravel beaches (McCall et al., 2014; 2015). The XBeach-G model can simultaneously simulate the transport of gravel sediments and groundwater flow. However, the applicability of this model to simulating a tsunami wave, gravel sediment transport by a tsunami, and groundwater flow induced by a tsunami has not been investigated. In addition, neither the gravel sediment transport model using XBeach (Jamal et al., 2014) nor XBeach-G

(McCall et al., 2014, 2015) has been extended for two-dimensional modelling and modelling of gravel sediment transport by a tsunami. Tsunami-induced sediment transport is significantly affected by three-dimensional topography (e.g., Abe et al., 2020). Thus, developing two-dimensional modelling that can predict gravel sediment transport is required.

This study extended the one-dimensional XBeach-G model to simulate two-dimensional gravel transport by a tsunami. To validate the extended XBeach-G model, the laboratory experiments conducted by Synolakis (1987) were first simulated to confirm the applicability of the XBeach-G model to simulating tsunami propagation and inundation. Hydrodynamics and gravel transport by the 2011 Tohoku-oki tsunami at Koyadori, Japan, were then modelled, and the observed distribution of gravel deposits was compared with the modelled distribution.

#### 2. Study area

Koyadori (39.4267° N, 142.0152° E), located in Iwate Prefecture, Japan, was selected as the study area (Fig. 1). The site was chosen specifically because of its distinctive valley-shaped topography, which significantly influences the behaviour of tsunamis. This unique three-dimensional terrain amplifies tsunami wave action, resulting in notable sediment transport processes. Previous research by Ishimura and Miyauchi (2015) identified evidence of 11 distinct tsunami events within the past 4000 years, each leaving behind characteristic layers composed of sand and gravel. These deposits highlight the area's long history of repeated tsunami-induced sedimentation events. Due to these factors, Koyadori is a suitable area to test and validate the extended gravel sediment transport model proposed in this study.

In Koyadori, the mouth of the valley is closed by a beach ridge (Fig. 2). The east side of the valley comprises Early Cretaceous hornblende-biotite granodiorite, granite, granite porphyry, and tonalite. The west side includes dacite, rhyolite lava, and pyroclastic rock deposited during the Early Cretaceous (Yoshida et al., 1984). The beaches in Koyadori are composed of gravel with a median sediment size  $D_{50}$  of 0.37 cm (Fig. 2d). Before the 2011 Tohoku-oki tsunami, the land slope at the site was roughly 0.0175 along the transect shown in Fig. 2. Behind the shoreline, there was a dune, approximately 5 m high, at the top of which a concrete coastal dike, with a crest height of 7 m above sea level at 75 m inland from the shoreline, had been constructed to protect the hinterland (Fig. 2c). This coastal dike was washed away by the 2011 Tohoku-oki tsunami. The dune extended up to 140 m inland from the shoreline, Behind the dune, about 150 m inland from the shoreline,

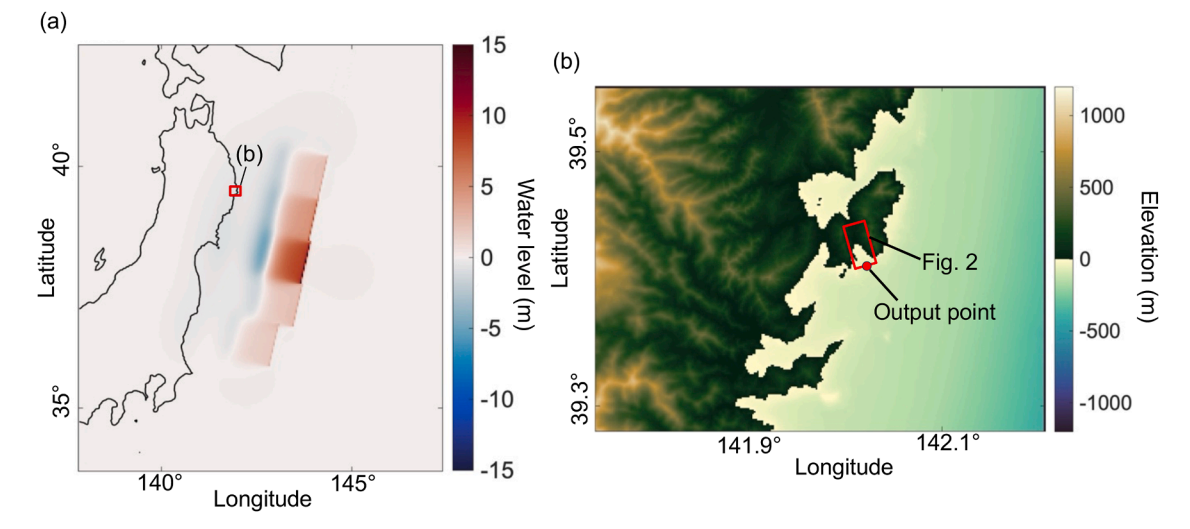


Fig. 1. (a) The initial wave height of the 2011 Tohoku-oki tsunami using the source model proposed by Imamura et al. (2012) and the location of the study area. (b) The location of Koyadori. The red square shows the numerical domain of the extended XBeach-G. The red circle is the output point of the time series of water levels by Delft3D.

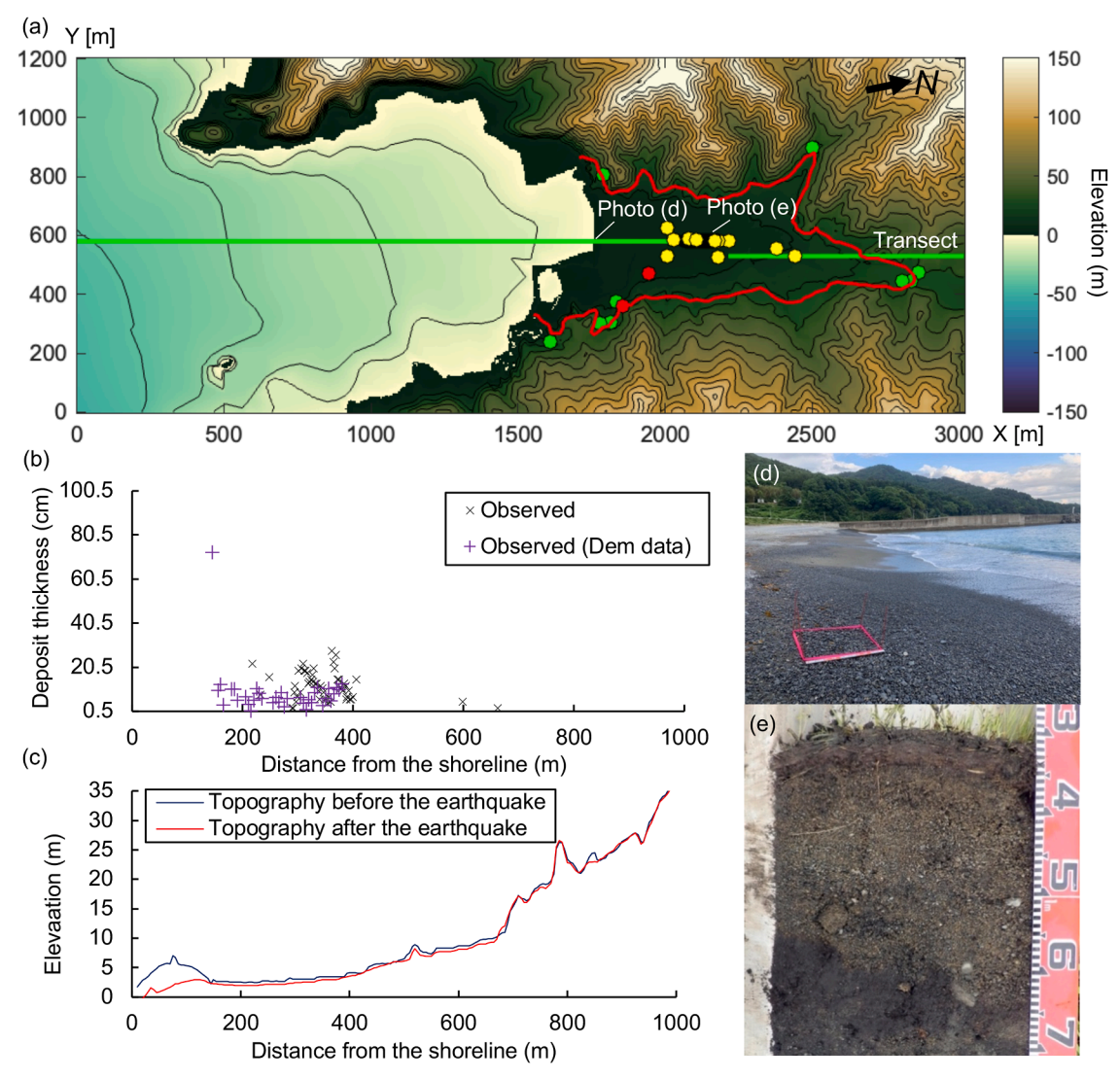


Fig. 2. (a) The topography and bathymetry in the numerical domain of the extended XBeach-G. The solid red line denotes the inundation line of the Tohoku-oki tsunami, as identified by Haraguchi and Iwamatsu (2011). The solid counter lines indicate the elevation of topography and bathymetry with an interval of 10 m. Yellow points indicate the pit locations in the gravel tsunami deposit surveys by Ishimura and Miyauchi (2015), Ishimura et al. (2015) and Ishimura and Yamada (2021). Green and red points are observation points of runup heights and water depth by Mori et al. (2011). At the location of Photo (d), the grain size of gravels in this study area was measured. (b) The measured thickness of gravel deposits formed by the 2011 Tohoku-oki tsunami (Ishimura and Miyauchi, 2015; Ishimura et al., 2015; Ishimura and Yamada, 2021) and the observed thickness of gravel deposits derived by subtracting the Digital Elevation Model (DEM) data surveyed in April 2011 from the DEM data surveyed in 2006. Both DEM data were supplied by the Geospatial Information Authority of Japan (2025b). (c) Cross-sectional topographies along the transect before the earthquake (DEM data surveyed in 2006) and after the earthquake (DEM data surveyed in April 2011). (d) Photograph of gravel beach at Koyadori. (e) Photograph of gravel deposits formed by the 2011 Tohoku-oki tsunami. This photo shows the uppermost part of the KYD-LGS4 core in Ishimura and Yamada (2021). The layer at 4 to 6 in the scale in this photo is the gravel layer formed by the 2011 Tohoku-oki tsunami. The locations of photographs (d) and (e) are indicated in (a).

there was a topographic depression due to a small river (Fig. 2c). Around 150-280 m behind the river, the land elevation was 2 m, and the land slope was almost zero. To the landward, there was a steep land slope from 280 m inland from the shoreline. At Koyadori, a land deformation of -0.56 m by the 2011 Tohoku-oki earthquake was observed (The Geospatial Information Authority of Japan, 2025a).

The observed maximum run-up height of the tsunami generated by the 2011 Tohoku-oki earthquake was 26.0–29.4 m at Koyadori, with maximum inundation depths ranging from 13 to 18 m (Haraguchi and Iwamatsu, 2011). The gravel layers formed by the tsunami were sourced from the beach and beach ridges and were carried up to 670 m inland from the coastline (Fig. 2b, e) (Ishimura and Miyauchi, 2015). The measured thickness of these deposits is 2–28 cm (Fig. 2b) (Ishimura and Miyauchi, 2015; Ishimura et al., 2015; Ishimura and Yamada, 2021). The roundness of gravel particles in tsunami deposits formed by the

2011 event was calculated using image analysis (Ishimura and Yamada, 2019), and the results showed that the gravels mainly consist of beach gravels.

To identify and analyse the spatial distribution of onshore gravel deposits that resulted from the 2011 Tohoku-oki tsunami, two sets of Digital Elevation Model (DEM) data (ASCII grid format) with a resolution of 2 m (the Geospatial Information Authority of Japan, 2025b) were compared (Fig. 2c). The first dataset was collected in 2006, before the tsunami event, while the second dataset was derived from aerial laser surveying conducted in April 2011, shortly after the tsunami occurred. To estimate the distribution of sediment deposits attributable to the tsunami, the 2006 DEM data were subtracted from the 2011 DEM data by assuming an average land deformation of  $-0.56\,\mathrm{m}$  in the study area. As a result, the distribution of sediment deposits from the shoreline up to 0.4 km inland could be estimated (Fig. 2). From 0.4 km inland from the

shoreline, reclamation work had been progressing after the 2011 earthquake. Thus, the onshore sediment distribution could not be estimated from 0.4 km inland. At 150 m inland from the shoreline, where the small river is located, a 70-cm layer of gravel deposited by the tsunami can be seen (Fig. 2b). However, the DEM data does not allow for an accurate estimation of gravel sediment thickness formed by the 2011 Tohoku-oki tsunami. For example, at 300-400 m inland from the shoreline, the deposit thickness obtained from the DEM data and thicknesses observed in the field (Ishimura and Miyauchi, 2015; Ishimura et al., 2015; Ishimura and Yamada, 2021) were not consistent (Fig. 2b). This is because the deposit thickness obtained from the subtraction of DEM data measured before and after the 2011 Tohoku-oki earthquake just quantified changes in elevation, meaning that thickness of deposit distributed over eroded bed is underestimated. Moreover, land deformation due to the earthquake in Kovadori is not uniform. Therefore, the DEM data was used to detect the location of sedimentation because it lacks the accuracy to determine the exact thickness of the deposits. To validate the simulation results of gravel sediment transport by the tsunami, the observed data on gravel tsunami deposits from Ishimura and Miyauchi (2015), Ishimura et al. (2015), and Ishimura and Yamada (2021) were utilised, as explained in Section 3.3.2.

#### 3. Method

#### 3.1. Numerical simulation models

This study extends the XBeach-G model to account for two-dimensional gravel sediment transport and bed level changes during a tsunami. For this, the open-source code of Xbeach-v.12.5527 (Deltares, 2015), which already contains the source code of XBeach-G was changed. In the XBeach-G model, intra-wave surface elevation and depth-averaged flow are solved using a non-hydrostatic extension of the non-linear shallow water equations (Smit et al., 2010) and a source term for the surface water–groundwater exchange flux (McCall et al., 2014). This enables the model to accurately simulate wave dispersion in intermediate to shallow water depths, as well as infiltration from surface water into the permeable gravel beach (McCall et al., 2014). Depth-averaged groundwater flow and the rate of exchange flow between the surface water and groundwater are solved using a turbulent flow extension of Darcy's Law (McCall et al., 2014; McCall, 2015).

The extended XBeach-G model accounts for two-dimensional surface water flow, groundwater flow, and bed level changes during gravel sediment transport by a tsunami, as outlined below. This study proposes two-dimensional gravel sediment transport and bed level changes, as described in Section 3.1.3.

# 3.1.1. Surface water flow

The low-frequency and mean flows are solved based on shallow water equations, including a source term for the surface water—groundwater exchange flux (S). Eqs. (1) and (2) are momentum equations in the x and y directions, and Eq. (3) represents continuity.

$$\frac{\partial u}{\partial t} + u \frac{\partial u}{\partial x} + v \frac{\partial u}{\partial y} - \nu_h \left( \frac{\partial^2 u}{\partial x^2} + \frac{\partial^2 u}{\partial y^2} \right) = \frac{\tau_{sx}}{\rho h} - \frac{\tau_{bx}}{\rho h} - g \frac{\partial \eta}{\partial x} + \frac{F_x}{\rho h} + \frac{F_{v, x}}{\rho h}, \tag{1}$$

$$\frac{\partial v}{\partial t} + u \frac{\partial v}{\partial x} + v \frac{\partial v}{\partial y} - \nu_h \left( \frac{\partial^2 v}{\partial x^2} + \frac{\partial^2 v}{\partial y^2} \right) = \frac{\tau_{sy}}{\rho h} - \frac{\tau_{by}}{\rho h} - g \frac{\partial \eta}{\partial y} + \frac{F_{v, y}}{\rho h} + \frac{F_{v, y}}{\rho h}, \tag{2}$$

$$\frac{\partial \eta}{\partial t} + \frac{\partial hu}{\partial x} + \frac{\partial hv}{\partial y} + S = 0, \tag{3}$$

where t is time, u and v represent the velocity in the x and y direction, respectively, f is the Coriolis coefficient,  $\rho$  is water density, h is the total water depth,  $\tau_{sx}$  and  $\tau_{sy}$  are the wind shear stresses in the x and y directions, respectively,  $\tau_{hx}$  and  $\tau_{hy}$  are the bed shear stress induced by the

stresses in the x and y direction, respectively, g is the gravitational acceleration,  $\eta$  is the surface water level,  $F_x$  and  $F_y$  are the wave-induced stresses in the x and y direction, respectively,  $F_{\nu, x}$  and  $F_{\nu, y}$  are the stresses caused by vegetation in the x and y directions, respectively. S is the surface water–groundwater exchange flux. The horizontal viscosity ( $\nu_h$ ) is computed by default using the Smagorinsky (1963) model to account for the exchange of horizontal momentum at spatial scales smaller than the computational grid size, as follows.

$$\nu_{h} = c_{S}^{2} 2^{\frac{1}{2}} \sqrt{\left(\frac{\delta u}{\delta x}\right)^{2} + \left(\frac{\delta v}{\delta y}\right)^{2} \frac{1}{2} \left(\frac{\delta u}{\delta x} + \frac{\delta v}{\delta y}\right)^{2}} \Delta x \Delta y, \tag{4}$$

where  $c_s$  the Smagorinsky constant. The typical range of  $c_s$  is 0.10 - 0.27, and  $c_s$  = 0.1 is proposed for open channel flow (Murakami, 1993). Thus,  $c_s$  was assumed to be 0.1 for modelling the storm waves over a gravel beach with XBeach-G (McCall et al., 2014) and 0.094 for solitary waves (Dimakopoulos et al., 2014). An approximate value of 0.1 has been used for  $c_s$  in these studies, thus this study assumed  $c_s$  = 0.1 for modelling the tsunami wave over the gravel beach.

#### 3.1.2. Groundwater flow

The Laminar flow of an incompressible fluid through a homogeneous medium can be described using the well-known Law of Darcy (1856).

$$u_{gw} = -K \frac{\partial \overline{H}}{\partial \mathbf{r}},\tag{5}$$

$$v_{gw} = -K \frac{\partial \overline{H}}{\partial \gamma},\tag{6}$$

where  $u_{gw}$  and  $v_{gw}$  are velocities of groundwater in the x and y directions, respectively, K is the hydraulic conductivity of the aquifer, and  $\overline{H}$  is the depth-averaged hydraulic head.

To calculate the value of K, the following equation was used:

$$K = \begin{cases} K_{lam} \sqrt{\frac{Re_{crit}}{Re}} & \text{if } Re > Re_{crit} \\ K_{lam} & \text{if } Re \leq Re_{crit} \end{cases}, \tag{7}$$

where  $K_{lam}$  is the laminar hydraulic conductivity, Re is the current Reynolds number of the interstitial flow, and  $Re_{crit}$  is the critical Reynolds number for the start of turbulent flow.

The vertical velocity at the groundwater surface  $(w_{gs,s})$  is computed from the gradient of Eq. (8) at the surface and the hydraulic conductivity. The groundwater level  $(\zeta_{gw})$  is subsequently calculated in Eq. (9).

$$w_{gs,s} = -2\beta h_{gw}K, \tag{8}$$

$$\frac{\partial \zeta_{gw}}{\partial t} + \frac{\partial h_{gw} u_{gw}}{\partial x} + \frac{\partial h_{gw} v_{gw}}{\partial y} - S = 0, \tag{9}$$

where  $h_{\rm gw}$  is the water depth of groundwater flow above the aquifer's bottom, and  $\beta$  is the parabolic curvature coefficient.

#### 3.1.3. Bed level changes during gravel sediment transport

According to Nielsen (2002), the total transport load of gravel sediments is calculated using a modification of the Meyer-Peter and Müller (1948) equation for bed load transport. The equation of the Meyer-Peter and Müller (1948) is as follows:

$$q_{tot} = C[(s-1)gD_{50}^3]^{1/2}(\theta - \theta_{cr})^{3/2}, \tag{10}$$

where  $q_{tot} = \left(q_{tot,x}, \ q_{tot,y}\right)$  is the total volumetric sediment transport rate.  $q_{tot,x}$  and  $q_{tot,y}$  are volumetric sediment transport rates in the x and y direction, respectively.  $\theta$  is the Shields parameter,  $\theta_{cr}$  is the critical Shields parameter, s is the submerged density of the sand particle, C is the multiplier, and  $D_{50}$  is the median sediment grain size.

The Shields parameter ( $\theta$ ) is computed using the following relation.

$$\theta = \frac{\frac{1}{2}f_s}{(s-1)gD_{s_0}}U_c^2,\tag{11}$$

where  $f_s$  is a user-defined sediment friction factor and  $U_c$  is the total velocity.

The critical Shields parameter ( $\theta_{cr}$ ) for the transport initiation is computed using the relation of Soulsby and Whitehouse (1997) as follows:

$$\theta_{cr} = \frac{0.3}{1.2 + D_*} + 0.055 (1 - e^{-0.020} D_*), \tag{12}$$

$$D_* = D_{50} \left(\frac{\Delta g}{\nu^2}\right)^{\frac{1}{3}},\tag{13}$$

where  $D_*$  is the non-dimensional grain size, and  $\nu$  is the kinematic viscosity coefficient of water.

The bed level changes are calculated as follows:

$$\frac{\partial z_b}{\partial t} + \frac{1}{(1-p)} \nabla \cdot q_{tot} = 0, \tag{14}$$

where,  $z_b$  is the bed level, and p is the sediment porosity. To introduce the effect of slope on the gravel sediment transport,  $\nabla \cdot q_{tot}$  in Eq. (14) is calculated as follows.

$$\nabla \cdot q_{tot} = \frac{\partial}{\partial x} \left( q_{tot,x} - \varepsilon \left| q_{tot,x} \right| \frac{\partial z}{\partial x} \right) + \frac{\partial}{\partial y} \left( q_{tot,y} - \varepsilon \left| q_{tot,y} \right| \frac{\partial z}{\partial y} \right), \tag{15}$$

where,  $\varepsilon$  is an empirical coefficient. The value of the coefficient was set at 2.0, as in Tanaka et al. (1989), and this also has a role in stabilising sediment transport calculation (e.g., Takahashi et al., 1992).

# 3.2. Validation of the tsunami simulation

The numerical simulation model was validated using Synolakis's experimental data (1987), which observed the wave shape and runup height over a uniform slope of a solitary wave, which has been used as a representative of a modelled tsunami wave (e.g., Madsen et al., 2008). The experimental data have been published as a benchmark test for validating tsunami simulation models (NOAA, 2025).

Synolakis (1987) investigated the runup characteristics of solitary waves over an impermeable uniform slope (Fig. 3) in a 40-m wave tank equipped with a piston-type wave maker. The tank was 37.73 m long, 0.61 m wide, and 0.39 m high. A sloping beach was constructed with a hydrodynamically smooth surface at a distance of 14.68 m from the wave generator. The slope angle was 1/19.85, and the water depth was 20 cm.

This study conducted a cross-sectional calculation of the experiment using the extended XBeach-G model. In the simulation, a solitary wave was input in the numerical domain using the following equation from Watanabe and Arikawa (2023):

$$\eta(x,t) = H \operatorname{sech}^{2}\left(\sqrt{\frac{3H}{4h^{3}}}\left(x - \sqrt{g(h+H)}t\right)\right),\tag{16}$$

where  $\eta(x,t)$  is water level, t is time, H is wave height, and h is water depth. The time interval was automatically determined based on the Courant number. Horizontally, grid cells of 0.01 m were used. In the simulation, Manning's roughness coefficient was assumed to be 0.0125  $\mathrm{m}^{-1/3}$  s because the topography was created using smooth materials. This study conducted simulations for two cases: one where wave breaking is not generated ( $\varepsilon=0.04$ ) and another where wave breaking is generated ( $\varepsilon=0.3$ ). The calculation time was set to be 120 s for both simulations.

The performance of the simulation was finally evaluated using the root-mean-square (RMSE) given by

$$RMSE = \sqrt{\frac{1}{N} \sum_{i=1}^{N} (x_{obs} - x_{cal})^{2}},$$
(17)

Therein,  $x_{obs}$  is the observed value,  $x_{cal}$  is the calculated value, N is the total number of data, and i is an index. In the case of a hypothetical perfect match between model and data, the RMSE should be zero. It can be concluded that the smaller the RMSE, the better the calculation's performance. The RMSE values were calculated to investigate whether observed dimensionless wave heights were reproduced in the numerical simulations.

# 3.3. Gravel transport by the 2011 Tohoku-oki tsunami at Koyadori

#### 3.3.1. Tsunami simulation with the extended XBeach-G

To simulate gravel transport by the 2011 tsunami using the extended XBeach-G, input data for the extended XBeach-G were obtained by calculating the time series of the water level offshore of Kovadori using Delft3D (Version 3.15) (Deltares, 2020), Delft-3D is an open-source code that implements the shallow water equations when applied with one vertical layer (Deltares, 2020). The setting of Delft-3D in this simulation was identical (though without sand transport) to the setting in Watanabe et al. (2018), where the simulated inundation depths reasonably reproduced the inundation depths observed after the 2011 Tohoku-oki tsunami (for a discussion of this result; see Watanabe et al. (2018). The Cartesian coordinate system was used for the Delft3D modelling. The model resolutions of Delft3D were 3645 m, 1215 m, 405 m, 135 m, 45 m, and 15 m in domains 1, 2, 3, 4, 5, and 6, respectively. Topographic data were generated from the pre-2011 earthquake DEM data, with a resolution of 2 m, which is published as raster data by the Geospatial Information Authority of Japan (2025b). The simulation was conducted using the topography from which the coastal dike was removed (Fig. 4), as the coastal dike behind the coastline had been washed away during the tsunami (the limitations of this calculation are discussed in Section 4.5). The bathymetry data were generated from high-density depth contour data (Japan Hydrographic Association, 2001) for the Tohoku region. The wave source of the tsunami was the composite fault model proposed by Imamura et al. (2012), which was made to reproduce the observed inundation area during the 2011 Tohoku-oki tsunami. The model is composed of 10 fault segments, each 100 km long and wide,



Fig. 3. A schematic diagram of a laboratory experiment by Synolakis (1987).

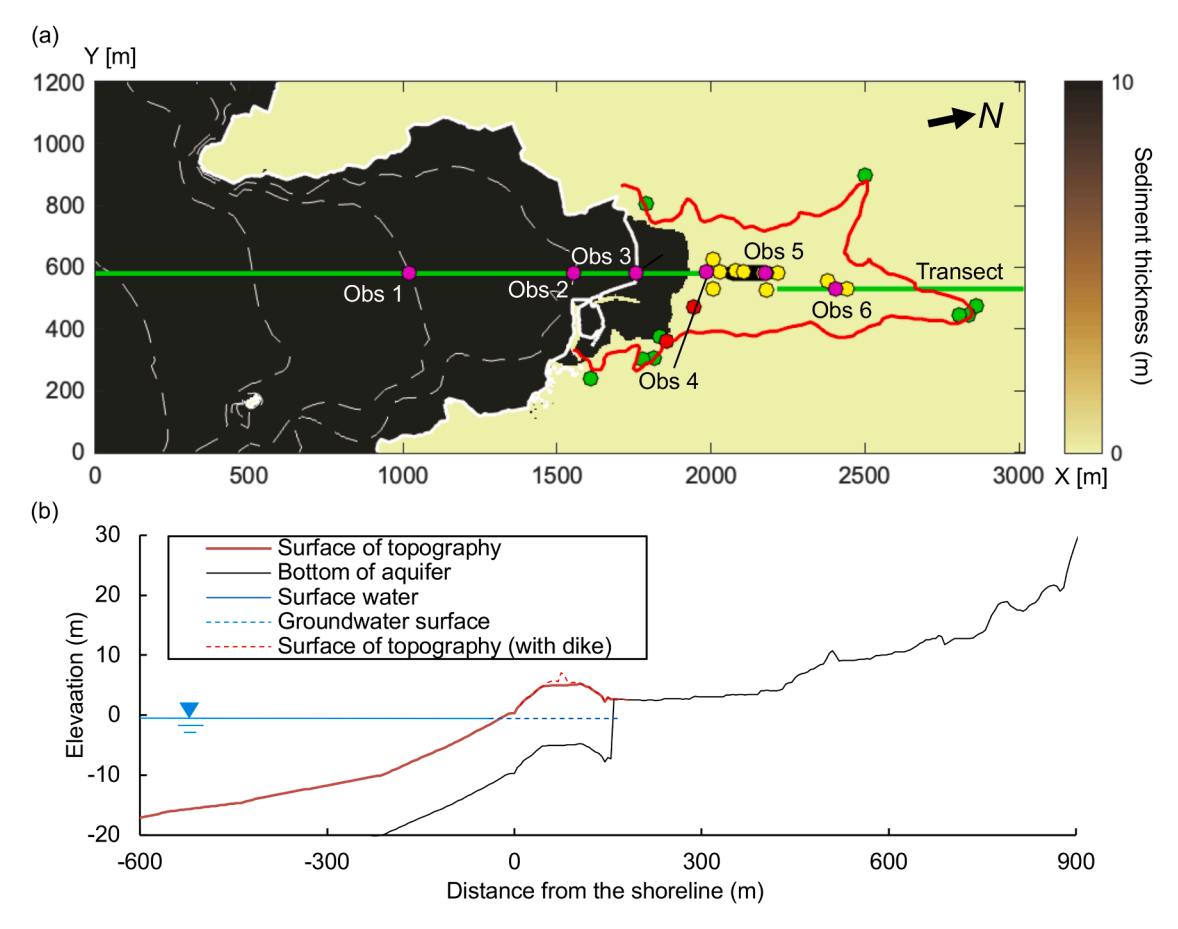


Fig. 4. (a) The initial thickness of gravel sediments before the simulation. The solid red line denotes the inundation line of the Tohoku-oki tsunami, as identified by Haraguchi and Iwamatsu (2011). The dotted counter lines indicate the elevation of -10 m, -20 m, and -30 m. The solid while line indicates the shoreline. Yellow points indicate the pit locations in the gravel tsunami deposit surveys by Ishimura and Miyauchi (2015), Ishimura et al. (2015) and Ishimura and Yamada (2021). Green and red points are observation points of runup heights and water depth by Mori et al. (2011). Obs 1–6 are the observation points of the gravel deposit thickness time series. (b) The topography, groundwater surface, and gravel layer surface along the transect before the simulation. Over the surface of topography, infiltration and exfiltration of groundwater occur. Below the bottom of the aquifer, water doesn't penetrate.

arranged along the Japan Trench in two rows (Fig. 1a). This tsunami source model was used to compare the simulation results of gravel sediment transport in this study and the calculated deposition process of sand and mud sediments by the 2011 tsunami using the same source model (Watanabe et al., 2023). The crustal deformation of the seafloor was calculated based on the elastic model proposed by Okada (1985), with the initial tsunami waveform assumed to be identical to it. The simulation was run for over five hours (18,000 s) to include the effects of both direct waves and reflected and refracted waves. The time series of water level at 700 m offshore from the coastline was then output (water depth: 47 m) (Fig. 1b).

The time series of water levels calculated by Delft3D was input into the offshore boundary of extended XBeach-G's numerical domain. Other boundaries are set as Neumann boundary conditions, but the inundated tsunami did not reach the boundaries, meaning that there is no boundary effect. The initial water level of the numerical domain was set at  $-0.56~\rm m$ , which corresponds to the observed land deformation at Koyadori caused by the 2011 Tohoku-oki earthquake (The Geospatial Information Authority of Japan, 2025a). For the simulation, Manning's roughness coefficients were set to be  $0.03~\rm m^{-1/3}$  s over the forest and  $0.025~\rm m^{-1/3}$  s over the beach, seafloor and artificial objects, such as paved surfaces given by Kotani et al. (1998). The calculation time was five hours, including the run-up flow and backwash effects. The Cartesian coordinate was used for the XBeach-G modelling. The grid cell resolution was set at 5 m. To validate the simulation results using the extended XBeach-G, the accuracy of the model was examined by

comparing the numerical results with water depths measured at Koyadori (Mori et al., 2011). The calculated inundation area was also compared with the observed one (Haraguchi and Iwamatsu, 2011).

### 3.3.2. Gravel transport simulation with the extended XBeach-G

The transect was set at the sites where Ishimura and Miyauchi (2015) surveyed the distribution of the gravel deposits (Fig. 2a) to compare measured and calculated results. The source of gravel in the simulation was from the seafloor to the beach dune (Fig. 4a), as indicated by grain size analysis (Ishimura and Miyauchi, 2015). From September to December 2011, after the 2011 Tohoku-oki earthquake occurred, drilling surveys were conducted at 75 m inland from the shoreline, where a coastal dike had been located before the earthquake, by the Miyako Agriculture and Forestry Promotion Centre of the Coastal Regional Development Bureau (personal communication). This survey investigated the subsurface section along a parallel to the coastline and revealed that the gravel sediment layers are 1-19 m thick at this site. Based on this survey result, the initial sediment layer thickness, which is the thickness of the movable bed in the modelling, was assumed to be 10 m (Fig. 4a). Below the 10-m depth from the topographic surface, the bottom of the aquifer was set (Fig. 4b). Below this aquifer, infiltration or exfiltration of groundwater does not occur.

Based on the measurements in this study (Section 2), the median grain size (D50) was set at 0.37 cm. The computed inland distribution distance of gravel sediment layers was defined as the distance from the shoreline to which sediments thicker than 5 mm were distributed,

following previous field and numerical works (e.g., Abe et al., 2012; Sugawara et al., 2014; Watanabe et al., 2021).

To validate the accuracy of the calculated onshore distribution of gravel tsunami deposits, this study used the deposited volume. This is because there are no topography and bathymetry datasets with a grid resolution of several centimetres in this study area. Onshore tsunami deposits are distributed with local fluctuation (e.g., Abe et al., 2020) and the deposit distribution is often controlled by the centimetre scale of onshore local depressions in the terrain (e.g., Takeda et al., 2018), meaning that there are uncertainties associated with the sediment thickness distribution, as a small change in the position of the measuring transect may alter the sediment thickness. Therefore, numerical simulation results of sediment transport by a tsunami have been validated by reproducing the general distribution trend (e.g., Sugawara et al., 2014) or deposit volume over land (e.g., Masuda et al., 2022).

As described in Section 2, the DEM data does not have the accuracy to reproduce the measured thickness of gravel sediments (Fig. 2b). Thus, to evaluate simulation accuracy, the calculated results were compared with the coring results of Ishimura and Miyauchi (2015), Ishimura et al. (2015), and Ishimura and Yamada (2021) which are available at 0.21–0.645 km from the shoreline where measured data of gravel sediments are continuously distributed (Fig. 2b). This study calculated deposit volume along the transect at 0.21–0.645 km from the shoreline, then compared this value with the measured values.

To understand the gravel transport process by the tsunami, a time series of water levels, velocities, and sedimentation and erosion of gravel layers was output at the six observation points. The observation points were set at the sites where water depths are 20 m (Obs 1), 10 m (Obs 2), and 0 m (Obs 3), near the starting point of measured gravel deposits (Obs 4, 215 m inland from the shoreline), at 405 m inland from the shoreline (Obs 5), and near the measured maximum extent of gravel deposits (Obs 6) (Fig. 4a).

# 3.3.3. Setting and sensitivity analysis of coefficients in gravel transport simulation

The hydraulic conductivity ( $K_{lam}$ ) values according to grain size have been summarised by McCall et al. (2015). For instance, previous research has indicated that a coarse gravel barrier with an average grain size of approximately 11 mm typically exhibits a hydraulic conductivity of around 155 mms<sup>-1</sup> (Williams et al., 2012; Turner and Masselink, 2012). Conversely, a fine gravel barrier with a grain size of approximately 2 mm typically has a much lower hydraulic conductivity of around 10 mms<sup>-1</sup> (Poate et al., 2013, 2014; Austin et al., 2013). For simulating gravel sediment transport in this study, the hydraulic conductivity ( $K_{lam}$ ) used in Eq. (7) was assumed to be 100 mms<sup>-1</sup>. The values of the sediment friction factor  $(f_s)$ , utilised in Eq. (11), and the multiplier (C), appearing in Eq. (10), were determined to ensure that the calculated onshore distribution of gravel tsunami deposits  $(R_d)$  are consistent with the observed values by changing these values. Previous research suggests sediment friction factor  $(f_s)$  values around the order of 0.01 (Masselink et al., 2014). Accordingly, the range of sediment friction factors was changed between 0.002 and 0.01 with an interval of 0.001. In some studies, the multiplier (C) has previously been assigned a value of approximately 12.0 (Masselink et al., 2014; Nielsen, 2002). However, Nielsen (2002) indicated different values for the multiplier depending on flow direction: 19.9  $\pm$  4.1 for uprush flow and 8.9  $\pm$  1.7 for downrush flow. Thus, the range of the multiplier was changed between 8.9 and 19.9 with an interval of 0.1. This study identified the best-fitted values within 999 combinations of the two parameters  $(f_s, C)$  through hyperparameter tuning. As a result, the simulated gravel sediment volumes along the transect closely matched the observed sediment volumes recorded in the field when  $f_s = 0.005$  and C = 13.6 as shown in Section 4.2 (Table 1).

This study then examined how variations in the hydraulic conductivity ( $K_{lam}$ ), the sediment friction factor ( $f_s$ ), and the multiplier (C) influence the model outputs. Using these reference values ( $f_s = 0.005$ , C = 0.005, C =

Table 1

Parameters used to simulate gravel sediment transport by the 2011 Tohoku-oki tsunami at Koyadori. Values in brackets represent the range of the parameter for the sensitivity analysis. The calculated volume of deposition ( $V_d$ ) and the ratio of the calculated deposition volume to the observation result ( $R_d$ ) when the setting parameters were used are shown.

$f_s$	$K_{lam}$	С	$V_d$	$V_{d\_obs}$	$R_d$
0.005 (0.002 - 0.01)	100 (0 - 155)	13.6 (8.9 - 19.9)	22.0	22.3	0.99
Symbols:					
$f_s$ ; Sediment friction factor					
K <sub>lam</sub> ; Laminar hydraulic conductivity (mms <sup>-1</sup> )					
C; Multiplier in the equation for gravel transport					
$V_d$ : The calculated volume of deposition (m <sup>2</sup> )					
$V_{d obs}$ ; The observed volume of deposition (m <sup>2</sup> )					
$R_{di}$ Ratio of the calculated deposition volume to the observation result					

13.6, and  $K_{lam} = 100 \, \mathrm{mms}^{-1}$ ), the sensitivity of the simulation results was further evaluated by varying each parameter individually and observing how the deposition volume along the transect responded to these parameter adjustments. For this analysis, the range of  $f_s$  was changed between 0.002 and 0.01 with an interval of 0.001, the range of C between 8.9 and 19.9 with an interval of 0.1, and the range of  $K_{lam}$  between 0.0 mms<sup>-1</sup> and 155 mms<sup>-1</sup> with an interval of 5.0 mms<sup>-1</sup> (Table 1).

### 4. Results and discussion

# 4.1. Numerical simulation of solitary wave run-up over the uniform slope

The comparison of the calculated result with the measured result of Synolakis (1987) is shown in Figs. 5 and 6. The measured results are displayed using dimensionless wave height (=H/h) and time  $(=t(g/h)^{1/2})$ . The XBeach-G model reproduced the wave height increase of a solitary wave due to shoaling (Fig. 5a, b) and the subsequent backwash (Fig. 5c, d). The propagation of a solitary wave was also reproduced when wave-breaking was generated (Fig. 6).

The *RMSE* values estimated from observed and calculated dimensionless wave heights are also shown in Figs. 5 and 6. In case wavebreaking is not generated ( $\epsilon=0.04$ ), the *RMSE* values were 0.0017–0.011 (Fig. 5). On the other hand, in case wave-breaking is generated ( $\epsilon=0.3$ ), the *RMSE* values were 0.010–0.018 (Fig. 6). In case wave-breaking is generated, the *RMSE* values became high because the XBeach-G model cannot directly solve wave breaking.

# 4.2. Numerical simulation of gravel transport by the 2011 Tohoku-oki tsunami at Koyadori

This section begins with a validation of the accuracy of the modelled gravel sediment transport during the tsunami event. As a result of parameter tuning of multiplier (C) and a sediment friction factor ( $f_s$ ), the calculated volume of gravel sediment deposits along the transect closely aligns with the measured values observed in the field when  $f_s = 0.005$  and C = 13.6 (Table 1). The sensitivity of the three parameters ( $f_s$ , C,  $K_{lam}$ ) are shown in Section 4.3.

Fig. 7 shows the calculated maximum water depth, current velocity during the tsunami, and gravel erosion and deposition after the tsunami (Table 1). The calculated maximum current velocity is 14.4 m/s at 310 m from the shoreline (X = 2085 m, Y = 485 m in Fig. 7). The calculated maximum water depth over the shoreline is 22.8 m. The calculated maximum inundation distance from the shoreline is consistent with the maximum inundation distance measured by Haraguchi and Iwamatsu (2011)

Behind the shoreline, water depth was measured by Mori et al. (2011) and the calculated values were 18.7 m and 17.7 m, respectively. The calculated water depth is consistent with the measured value, which was slightly underestimated. This is because the splash of the wave affects the field observation of the maximum water level (e.g., Sugawara

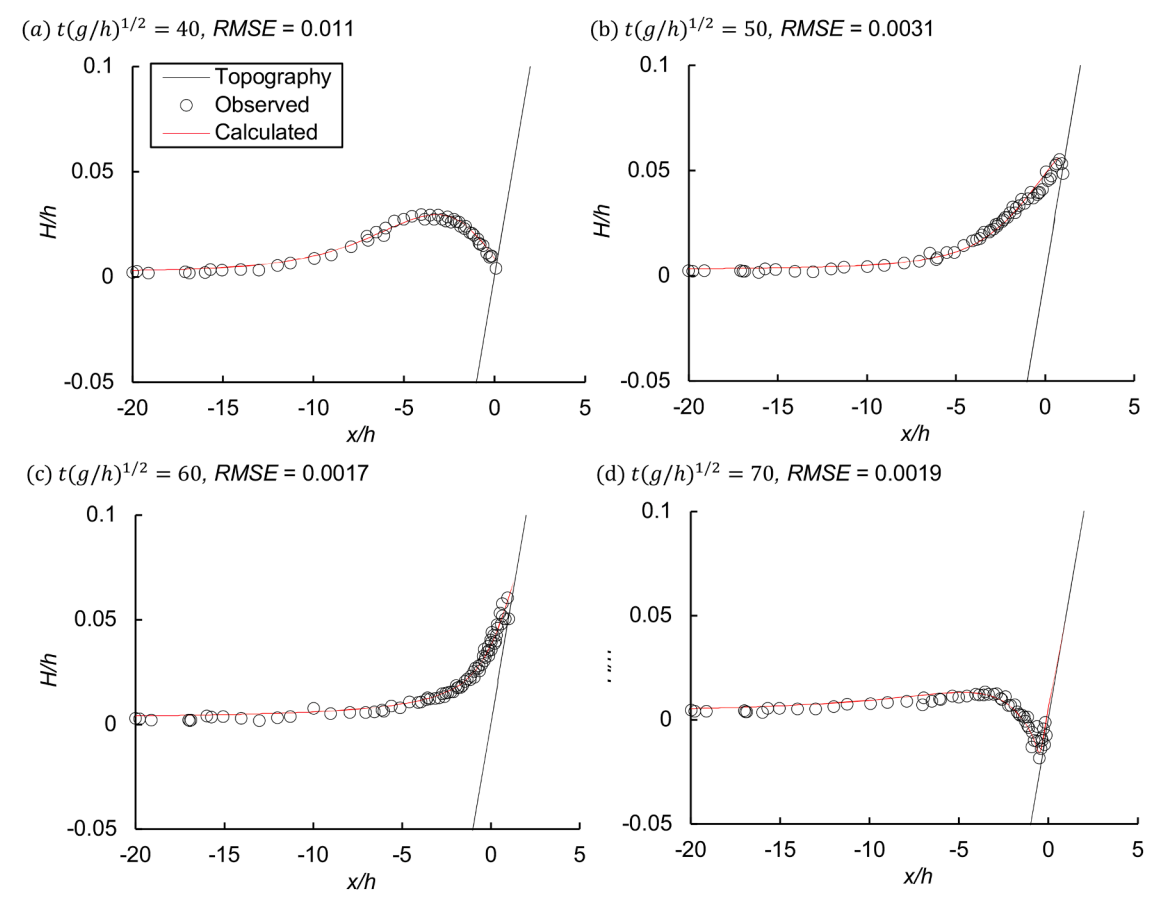


**Fig. 5.** Comparison of the observed and calculated values for spatial and temporal waveforms when a non-breaking solitary wave ( $\varepsilon = 0.04$ ,  $\varepsilon = H/h$ ) acts on a slope. H is wave height, and h is water depth. The results when (a)  $t(g/h)^{1/2} = 40$ , (b)  $t(g/h)^{1/2} = 50$ , (c)  $t(g/h)^{1/2} = 60$ , and (d)  $t(g/h)^{1/2} = 70$ . Therein, t is elapsed time, and g is gravitational acceleration.

et al., 2014; Watanabe et al., 2018), whereas the splash is not reproduced in the simulation.

The proposed model does not consider the washing away of the coastal dike at Koyadori (Section 2). When a tsunami simulation was conducted by removing the coastal dike, the maximum inundation depth along the transect decreased (Fig. 8c). At 845 m inland from the shoreline, the maximum water level when the coastal dike was not removed is 1.05 m lower than the calculated maximum water level when the coastal dike was removed (Fig. 8c). Therefore, if the washing away of the dike could be calculated simultaneously with gravel transport, the accuracy of the calculated water depth and inundation area would increase.

The calculated thickness of gravel sediments is highest at 0.145 km inland from the shoreline, where there is a minor local depression created by a stream (Fig. 8a). At this site, the DEM data shows the highest sediment thickness as well, owing to the concentration of gravel sediments. In the studies of Ishimura and Miyauchi (2015), Ishimura et al. (2015), and Ishimura and Yamada (2021), the measured maximum thickness of gravel deposits along the transect at 0.21-0.645 km from the shoreline was 26 cm at 0.369 km inland from the shoreline. This is consistent with the calculated thickness of 25.0 cm at 0.37 km inland from the shoreline. However, comparisons between simulated and observed thickness on a point-by-point basis are challenging, even though the overall trends agree well. The results indicate that the calculated deposits extended as sand sheets up to 755 m from the coast along the transect, while the observed deposits extended up to 662 m. This discrepancy is due to the locally formed sediments in a low-lying depression, and the local vegetation that traps sediments is not considered in the simulation. Thus, sediments with small layer thicknesses are

easily distributed inland in a numerical simulation, and similar results have been confirmed in previous studies (e.g., Watanabe et al., 2017).

When the tsunami reaches the shoreline (t = 22 min), sediment transport is mainly generated in the area where the water depth is <30 m (Fig. 9f). When t = 24 min, the maximum transport flux was 0.18 m<sup>2</sup>/s at 0.145 km from the shoreline (Fig. 9g). During the backwash when t =27 - 30 min, the gravel transport rate increased in Obs 3 (Fig. 9j), meaning that significant gravel transport occurred near the shoreline at this time. Then, significant sedimentation occurred near the shoreline after the backwash (Fig. 9n). To clearly illustrate the processes of erosion and sediment deposition induced by tsunami inundation, the results of vertical groundwater flow velocity, sediment transport rate, and updated topographic changes along the transect are presented in Fig. 10. At the initial moment when the tsunami wave reaches the shoreline, groundwater flow generates distinct vertical velocities along the transect, characterised by negative values (indicating downward infiltration of water into the sediment) and positive values (indicating upward exfiltration of groundwater) (Fig. 10a, b). As the tsunami inundates inland beyond the dune crest, the sediment transport rate becomes particularly significant between 50 m and 200 m inland from the shoreline (Fig. 10c, d). After that, the strong backwash flows led to noticeable alterations in the topography around the dune crest (Fig. 10g,

At Obs 4, gravel deposition started 21.5 min after the simulation began (Fig. 11d). After that the maximum gravel thickness was calculated, erosion and deposition started due to backwash, and the erosion and sedimentation finished 255 min after the start of the simulation. Thus, gravel deposition took 233.5 min. Deposition of the gravel deposits at Obs 6 started 23.5 min after the initiation of the simulation and

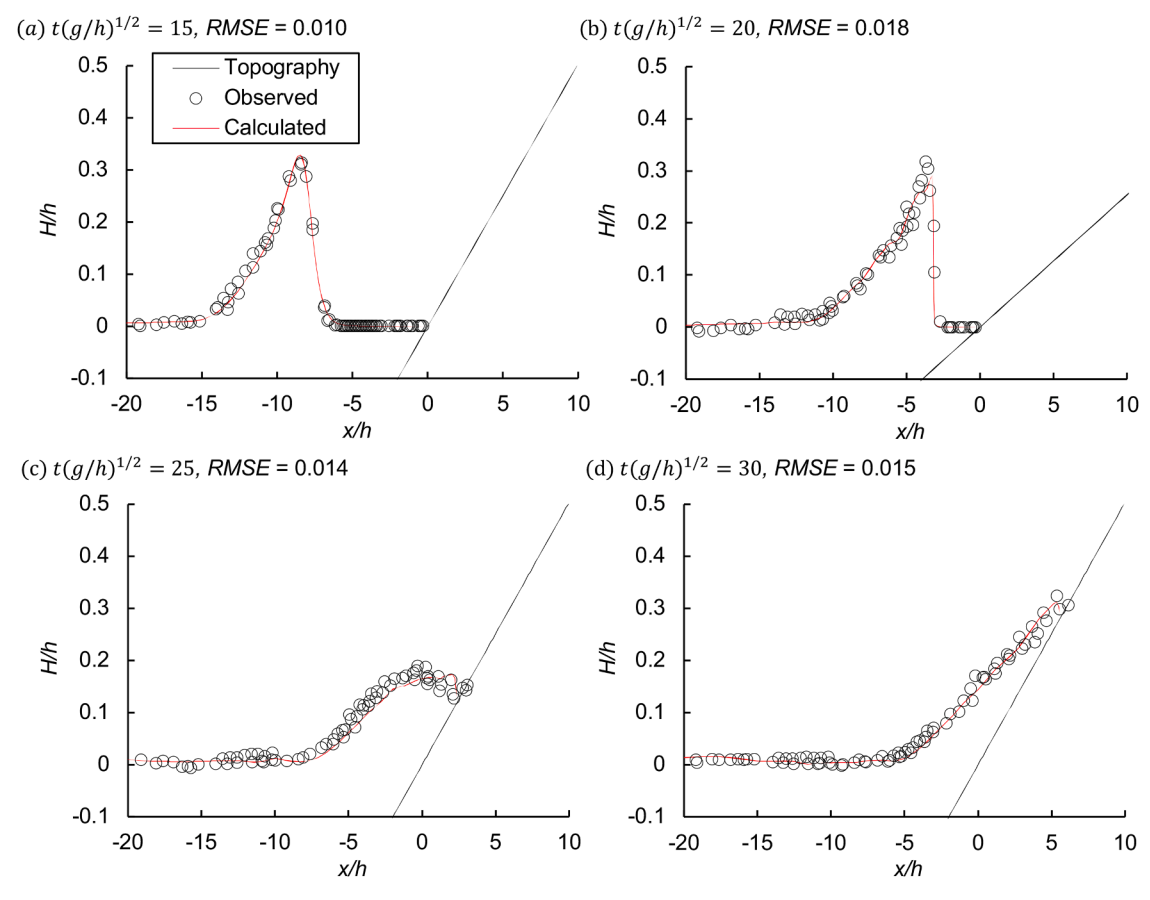


**Fig. 6.** Comparison of the observed and calculated values for spatial and temporal waveforms when a breaking solitary wave ( $\varepsilon = 0.3$ ,  $\varepsilon = H/h$ ) acts on a slope. H is wave height, and h is water depth. The results when (a)  $t(g/h)^{1/2} = 15$ , (b)  $t(g/h)^{1/2} = 20$ , (c)  $t(g/h)^{1/2} = 25$ , and (d)  $t(g/h)^{1/2} = 30$ . Therein, t is elapsed time, and g is gravitational acceleration.

finished 133 min after the start of the simulation (Fig. 11f). Thus, gravel deposition took 109.5 min. The deposition duration differed because the current of the tsunami was influenced by three-dimensional topography. Deposition time depends on the number of waves following the first tsunami wave. In the case of sand sediment transport by the 2011 Tohoku-oki tsunami in Sendai Plain, Japan (Watanabe et al., 2023a) with fewer subsequent tsunami waves, sediment deposition took 15.7 -23.2 min for sand sediment and 172 - 332 min for mud sediment. However, it is important to recognise that these sediment deposition times depend on the specific tsunami source model chosen to represent the 2011 Tohoku-oki tsunami. This study utilised the tsunami source model proposed by Imamura et al. (2012), which was calibrated primarily based on the observed tsunami inundation area. If an alternative source model had been employed—for example, the model proposed by Sugino et al. (2013), which was calibrated using observed offshore tsunami waveforms-the predicted deposition time could potentially differ.

# 4.3. The sensitivity analysis of the parameters used in the extended XBeach-G model

When the optimal parameter values ( $f_s = 0.005$ , C = 13.6, and  $K_{lam} = 100\,$  mms<sup>-1</sup>) was used, but the sediment friction factor ( $f_s$ ) or the multiplier (C) were systematically varied, a range of calculated-to-observed sediment deposition ratios ( $R_d$ ) was 0.20–1.67 for variations in  $f_s$ , and 0.59–1.87 for variations in C (Fig. 12). increasing the multiplier (C) resulted in consistently higher values of  $R_d$ . When  $f_s$  Increased beyond this value (greater than 0.007), the value of  $R_d$  decreased. This reduction occurred because higher friction factors facilitated greater sediment transport offshore during the backwash phase, subsequently

reducing the sediment available for deposition along the transect. Because of this backwash process,  $R_d$  was not higher than 2.15 in any parameter settings (Fig. 12). When hydraulic conductivity ( $K_{lam}$ ) was varied, the range of  $R_d$  was between 0.84 and 1.19 (Fig. 12c). The lowest value of  $R_d$  occurred when  $K_{lam}$  was set to 0.0 mms<sup>-1</sup> (indicating no groundwater flow calculation). For  $K_{lam}$  values between 10 mms<sup>-1</sup> and 155 mms<sup>-1</sup>,  $R_d$  values remained nearly constant, indicating that within this range, variations in  $K_{lam}$  had only a minor influence on sediment deposition. When groundwater flow was not modelled ( $K_{lam} = 0.0$ mms<sup>-1</sup>), the computed maximum water levels along the transect between -200 m and 0 m from the shoreline were higher compared to scenarios where groundwater flow was modelled ( $K_{lam} = 100 \text{ mms}^{-1}$  and  $K_{lam} = 155 \text{ mms}^{-1}$ ) (Fig. 8c). This difference occurs due to infiltration, as water entering among the gravel sediments reduces surface water levels. However, at locations further inland from the shoreline, the scenario reversed: the calculated maximum water levels when  $K_{lom} = 100 \text{ mms}^{-1}$ and  $K_{lam} = 155 \text{ mms}^{-1}$  exceeded those for the no-groundwater-flow scenario ( $K_{lam} = 0.0 \text{ mms}^{-1}$ ) (Fig. 8c). This increase inland is attributed to groundwater exfiltration, as groundwater emerges onto the surface, adding to inundation depth. For example, at 30 m inland from the shoreline, the maximum water level computed for  $K_{lam} = 100 \text{ mms}^{-1}$ was 0.77 m higher than the no-groundwater-flow case ( $K_{lam} = 0.0$ mms<sup>-1</sup>). Therefore, when groundwater flow is modelled, additional water can inundate inland areas through groundwater exfiltration, subsequently facilitating increased sediment transport inland. This explains why the deposition ratio  $(R_d)$  is lower when groundwater flow is not modelled ( $K_{lam} = 0.0 \text{ mms}^{-1}$ ) compared to scenarios where groundwater flow is included ( $K_{lam} = 100 \text{ mms}^{-1}$  and  $K_{lam} = 155 \text{ mms}^{-1}$ ) (Fig. 8c).

Tsunami inundation models and associated sand sediment transport

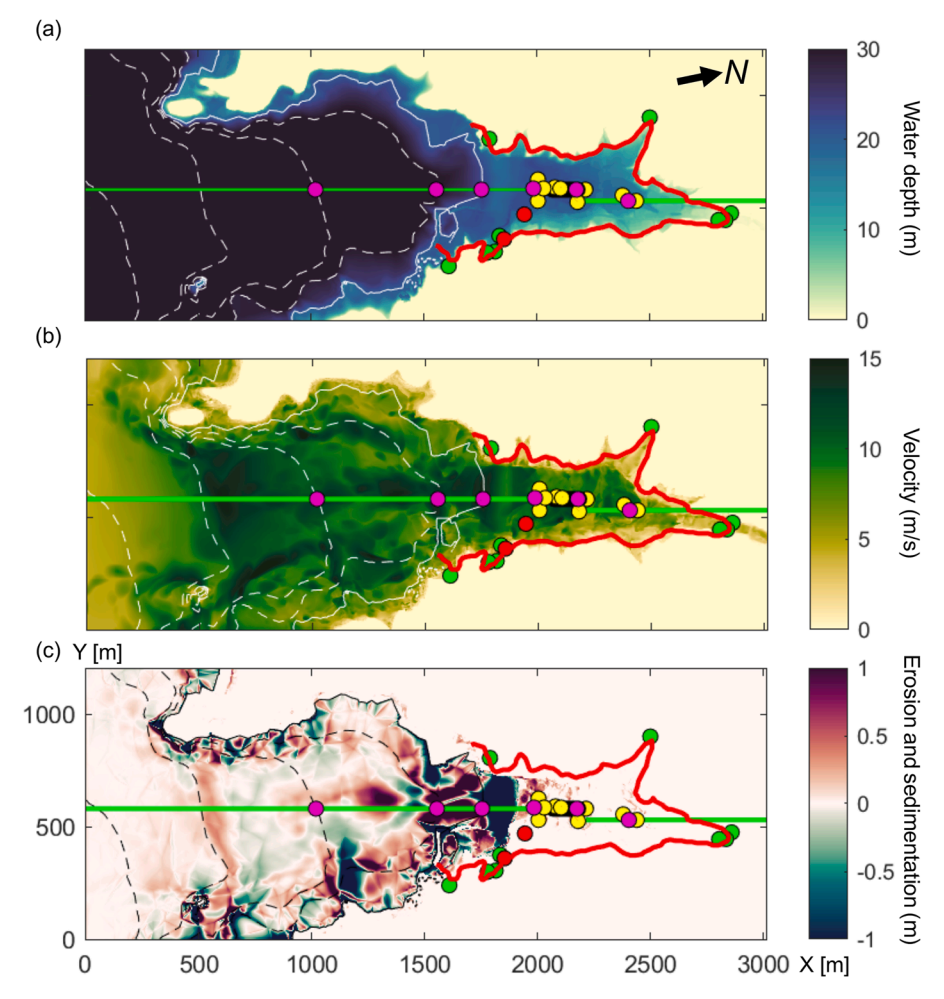


Fig. 7. The calculated (a) maximum water depth, (b) maximum current velocity, and (c) erosion and deposition of gravel sediments after the simulation by the extended XBeach-G. The solid red line denotes the inundation line of the 2011 Tohoku-oki tsunami, as identified by Haraguchi and Iwamatsu (2011). The white and black dotted counter lines indicate the elevation of -10 m, -20 m, -30 m, and -40 m, and the white and black solid lines indicate the shoreline. The green line is the transect set in this study. The pink points indicate the observation points where the time series data in Figs. 9 and 11 were output.

models have typically neglected groundwater flow processes. The results in this study clearly demonstrate that including groundwater flow is crucial, not only for accurately simulating tsunami inundation over gravel beaches but also for predicting gravel sediment transport. Nonetheless, despite this demonstrated importance, the overall impact of changing the value of  $K_{lam}$  (range: 0 to 155 mms<sup>-1</sup>) on deposition ratio (R<sub>d</sub>) remains relatively small compared to changes in the sediment friction factor  $(f_s)$  and the multiplier (C) (Fig. 12). Previous research has indicated that infiltration and exfiltration of water through sediment particles strongly influence gravel sediment transport under storm-wave conditions (e.g., Austin and Masselink, 2006; Horn and Li, 2006; Jamal et al., 2014). For instance, Jamal et al. (2014) demonstrated significant improvements in gravel beach profile modelling accuracy when accounting for infiltration and exfiltration processes. However, storm-generated waves typically have relatively short wavelengths (< 300 m), whereas tsunami waves have significantly longer wavelengths than storm waves. Thus, storm waves are readily attenuated by infiltration and exfiltration processes, whereas the extremely long wavelengths associated with tsunamis are not significantly affected by these processes when passing over gravel beaches.

#### 4.4. Application of the extended XBeach-G model

The runup and propagation of storm waves over gravel beaches, as well as the morphological changes of gravel beaches induced by storm

surge and waves, have been studied (e.g., Austin et al., 2006, 2013; Masselink et al., 2014; McCall et al., 2014, 2015; Poate et al., 2013, 2016). The proposed model of gravel transport, validated by the simulation of gravel transport at Koyadori, can be applied to estimate the thickness of gravel sediment deposition or the extent of coastal erosion caused by a tsunami. Previous studies have reconstructed paleotsunami events by determining the size of these historical tsunamis through numerical simulations that replicate observed distributions of sediment deposits (e.g., Sugawara et al., 2019). Although gravel tsunami deposits have frequently been documented in prior research (e.g., Moore, 2000; Nichol et al., 2003; Szczuciński et al., 2012; Yamada et al., 2014; Ishimura and Miyauchi, 2015; Inoue et al., 2017), such deposits have not yet been extensively used to estimate paleotsunami magnitudes. With the implementation of the gravel sediment transport model proposed in this study, gravel tsunami deposits, which are especially abundant in high-latitude regions or coral reef islands, can now effectively contribute to reconstructing historical tsunami magnitudes. If mud, sand, and gravel sediments and boulders formed by a paleotsunami were used for the reconstruction of the paleotsunami at the same time, the source of the paleotsunami can likely be strongly constrained. Consequently, the developed model enhances the understanding of historical tsunami risks and recurrence intervals. In this study, a two-dimensional model of gravel sediment transport by a tsunami was proposed. The development of a three-dimensional model will be necessary in the future, but the advantage of a two-dimensional model is that the computational load is

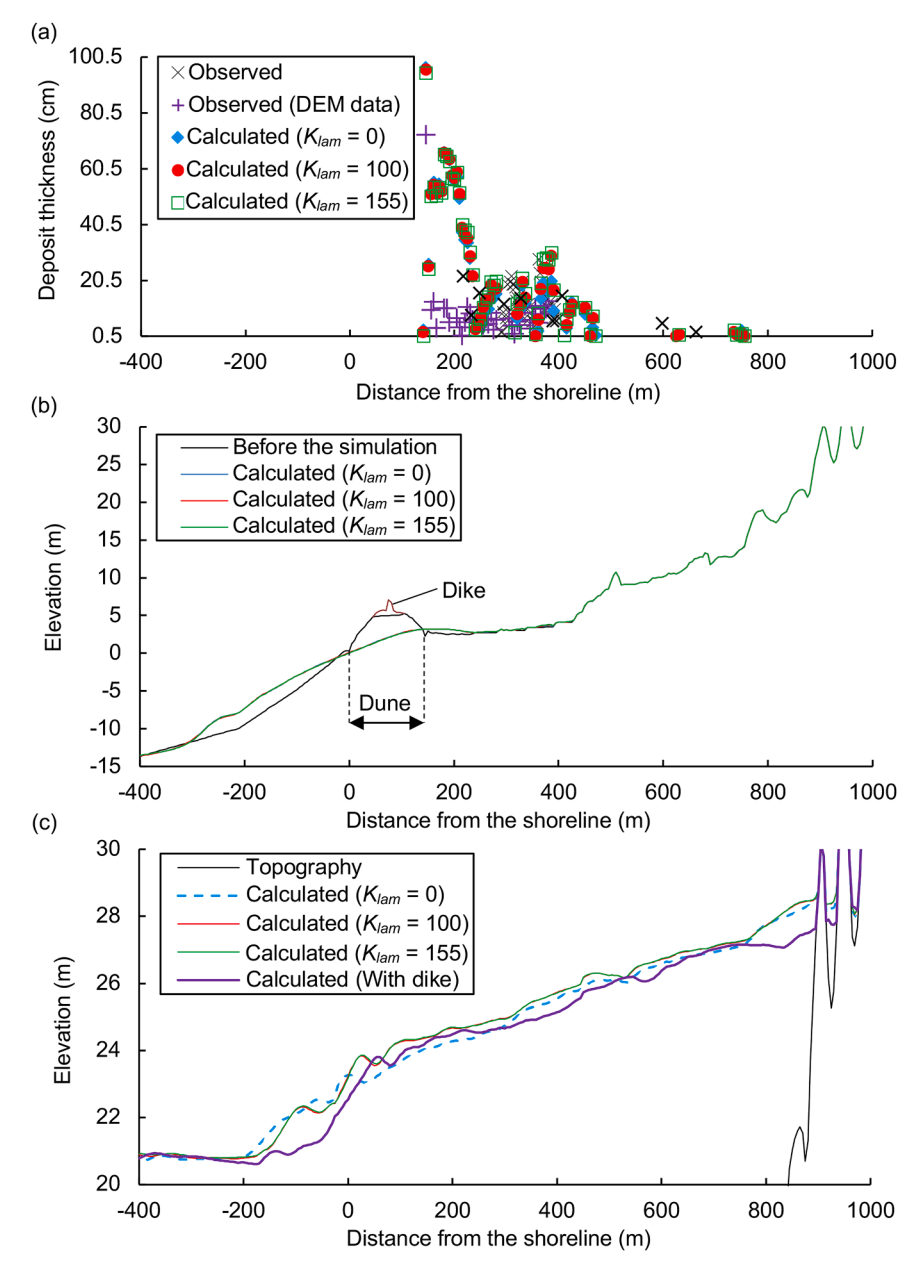


**Fig. 8.** (a) The measured thickness of gravel deposits formed by the 2011 Tohoku-oki tsunami (Ishimura and Miyauchi, 2015; Ishimura et al., 2015; Ishimura and Yamada, 2021) and calculated gravel layer thickness when  $K_{lam} = 0 \text{ mms}^{-1}$ ,  $K_{lam} = 100 \text{ mms}^{-1}$ , and  $K_{lam} = 155 \text{ mms}^{-1}$  along the transect. (b) Cross-sectional topographies along the transect before and after the simulations when  $K_{lam} = 0 \text{ mms}^{-1}$ ,  $K_{lam} = 100 \text{ mms}^{-1}$ , and  $K_{lam} = 155 \text{ mms}^{-1}$ . (c) The calculated maximum water levels along the transect when  $K_{lam} = 0 \text{ mms}^{-1}$ ,  $K_{lam} = 100 \text{ mms}^{-1}$ , and  $K_{lam} = 155 \text{ mms}^{-1}$ . The calculated water level when the coastal dike was not removed is also shown.

low, making the developed model more straightforward to use.

# 4.5. Limitations and future directions

This study developed a numerical simulation model of gravel sediment transport by a tsunami by extending the XBeach-G model; however, some issues require further investigation. One limitation of this study is that the proposed model and the setting parameters ( $f_s = 0.005$ ,  $K_{lam} = 100 \ \mathrm{mms^{-1}}$ , C = 13.6) were validated using one field dataset. The values of parameters could vary with sediment properties and the land surface environment. To further improve the proposed modelling method across diverse coastal environments, the model should be validated using various field observation data at various coastal settings.

In contrast, the field datasets are subject to many uncertainties. As discussed in Section 3.3.2, small-scale variations in topography or

vegetation can affect the distribution distance and thickness of gravel sediments. Therefore, further validation using laboratory experiment datasets is necessary. This study assumed a uniform 10-meter-thick mobile gravel layer for simulating gravel sediment transport. Thus, the effect of spatial gravel sediment layer thickness on gravel sediment transport requires further investigation. A laboratory experiment of tsunami propagation over gravel beaches under the condition that groundwater flow is generated has not been conducted. Thus, this phenomenon should be investigated based on physical modelling, and then the model should be upgraded to ensure that it can reproduce observed groundwater flow caused by a tsunami in a laboratory experiment to enhance the accuracy of predicting gravel sediment transport by a tsunami. The setting parameters were determined using the dataset of onshore gravel tsunami deposit thickness; therefore, erosion of the gravel beach was not considered for validation. For further validation, a

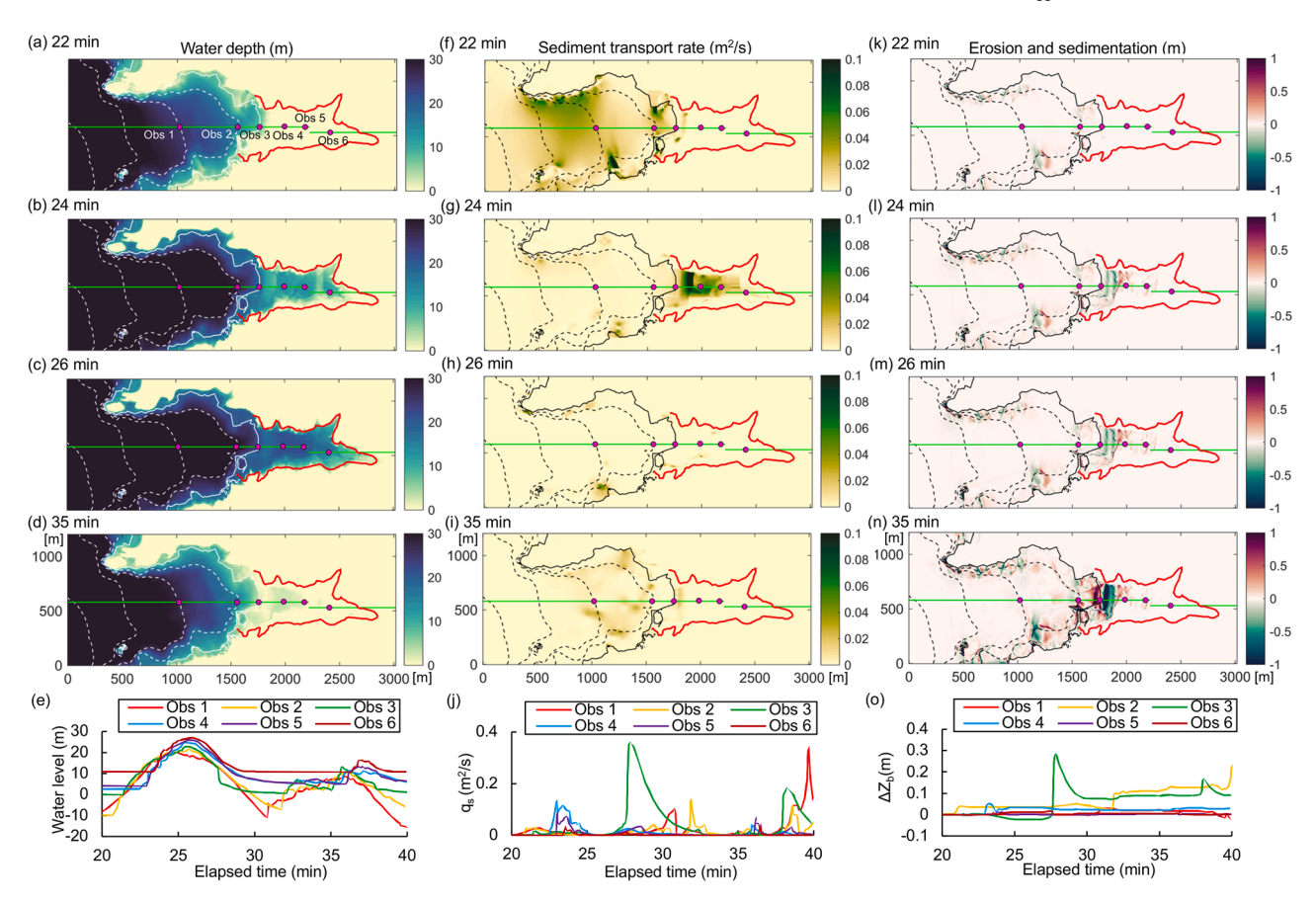


Fig. 9. The calculated water depths at (a) 22 min (when the tsunami reached the shoreline), (b) 24 min, (c) 26 min (when the tsunami reached its maximum inland inundation extent), and (d) 35 min (during backwash); gravel sediment transport rate at (f) 22 min, (g) 24 min, (h) 26 min, and (i) 35 min; and deposition and erosion of gravel layers at (k) 22 min, (l) 24 min, (m) 26 min, and (n) 35 min after the start of the simulation. The white and black dotted counter lines indicate the elevation of -10 m, -20 m, -30 m, and -40 m, and the white and black solid lines indicate the shoreline. The green line is the transect set in this study. The pink points indicate the observation points where time series data were output. The time series of (e) water levels, (j)  $q_s$  (gravel sediment transport rates), and (o)  $\Delta Z_b$  (erosion and sedimentation) at Obs 1–6 were also shown.

dataset of erosion and deposition profiles of gravel beaches caused by a tsunami should be collected. Various laboratory experimental data should also be used to validate the proposed model to further enhance the general applicability and credibility of the proposed modelling method across diverse coastal environments.

Smoothed particle hydrodynamics (SPH) can also likely simulate gravel transport by a tsunami. In the SPH model, fixed computational grids are not required when calculating spatial derivatives, making it suitable for solving tsunami–structure interactions (Huang and Zhu, 2015). However, the accuracy of SPH models is relatively lower compared to nonlinear shallow water equations (Watanabe et al., 2022). Moreover, SPH models especially suffer from longer simulation times than the nonlinear shallow water equations and require high-performance computers. Therefore, if gravel sediment transport simulation is to be used widely to understand the impact of tsunamis on the morphological dynamics of gravel beaches, the development of two-dimensional gravel transport models should be prioritised.

The calculation of only bedload is common in gravel transport simulations for river flows (e.g., Bellos and Hrissanthou, 2003; Van and Chua, 2020; Hsu and Hsu, 2022) and storm surges (e.g., McCall et al., 2014; 2015). Given that the maximum velocities of river flows are 2–3 m/s (Van and Chua, 2020) compared to observed tsunami velocities during the 2011 Tohoku-oki tsunami such as 8.0 m/s (Hayashi and Koshimura, 2013) or 11 m/s (Fritz et al., 2012), it is not clear whether both bedload and suspended load should be calculated, since during tsunami flow velocities, gravel particles are likely transported in suspension. The median sediment size in this study area is 0.37 cm; if the

sediment size is <0.37 cm, many gravel sediments may be transported as suspended load. To date, laboratory experiments on the transport of gravel sediment by a tsunami have not been conducted. Total gravel sediment transport was modelled by using the Meyer-Peter and Müller (1948) equation in this study. To improve the model accuracy, bedload transport and suspended transport loads of gravel sediments caused by a tsunami should be observed. Based on laboratory experiments, an equation that can reproduce the transportation flux of gravel particles during a tsunami should be proposed.

In this study, uniform sediment size and porosity were assumed. As natural gravel beaches often exhibit heterogeneity in grain size distribution, the effect of grain size distribution on deposition, erosion, and transportation of gravel sediments also needs to be investigated in the future. Understanding the factors that influence the onshore distribution of gravel tsunami deposits (e.g., tsunami intensity, water level changes due to tides, source of sediment, sediment properties) is essential for reconstructing the intensity of paleotsunami events from the gravel deposits; thus, this should be clarified in the future. The coastal dike was removed before the simulation in this study. If the failure of the coastal dike could be simulated with a tsunami propagation and gravel sediment transport, the simulation accuracy would increase. These issues need to be solved to enhance the accuracy of modelling gravel sediment transport by a tsunami.

#### 5. Conclusion

This study presented a new model to simulate gravel transportation

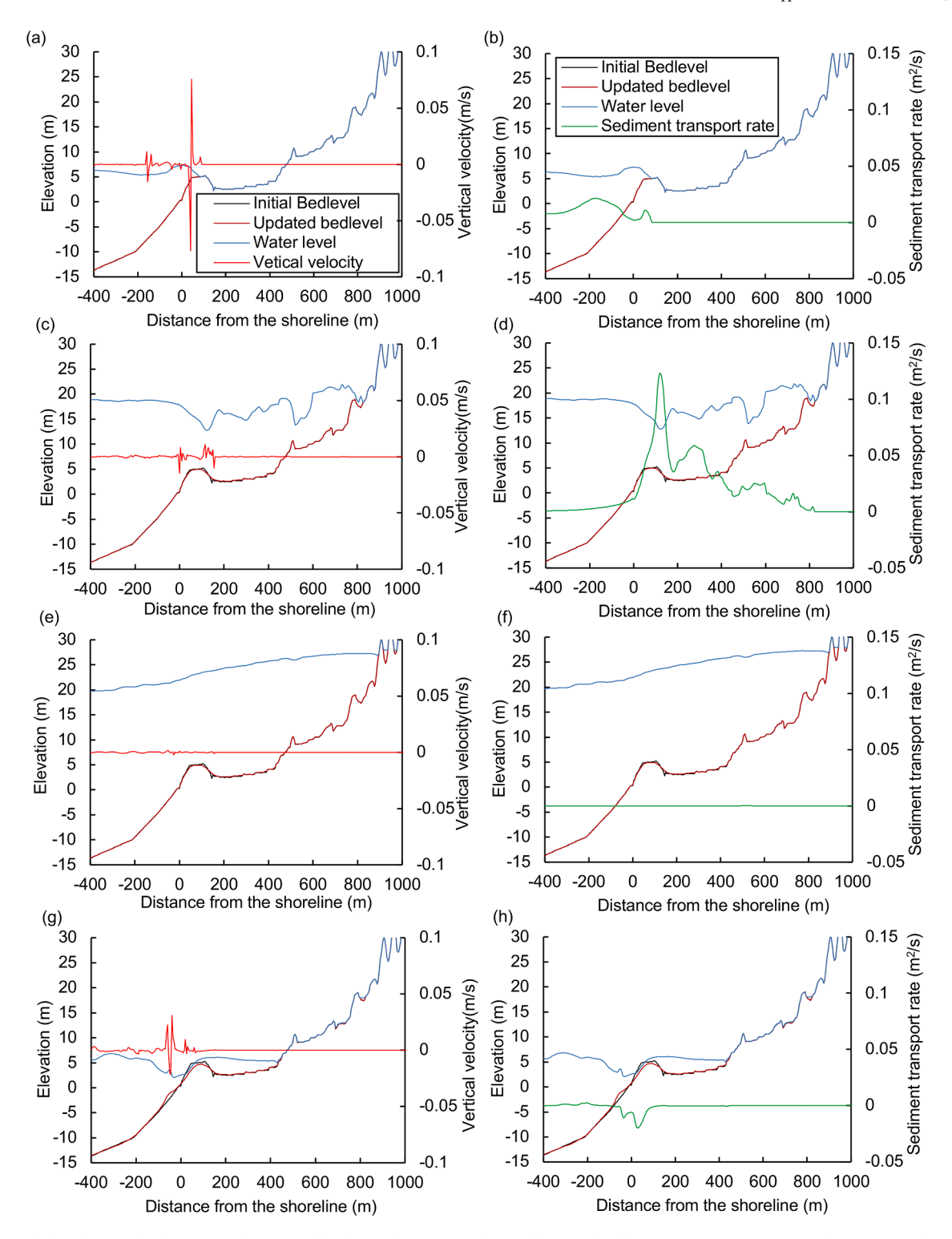
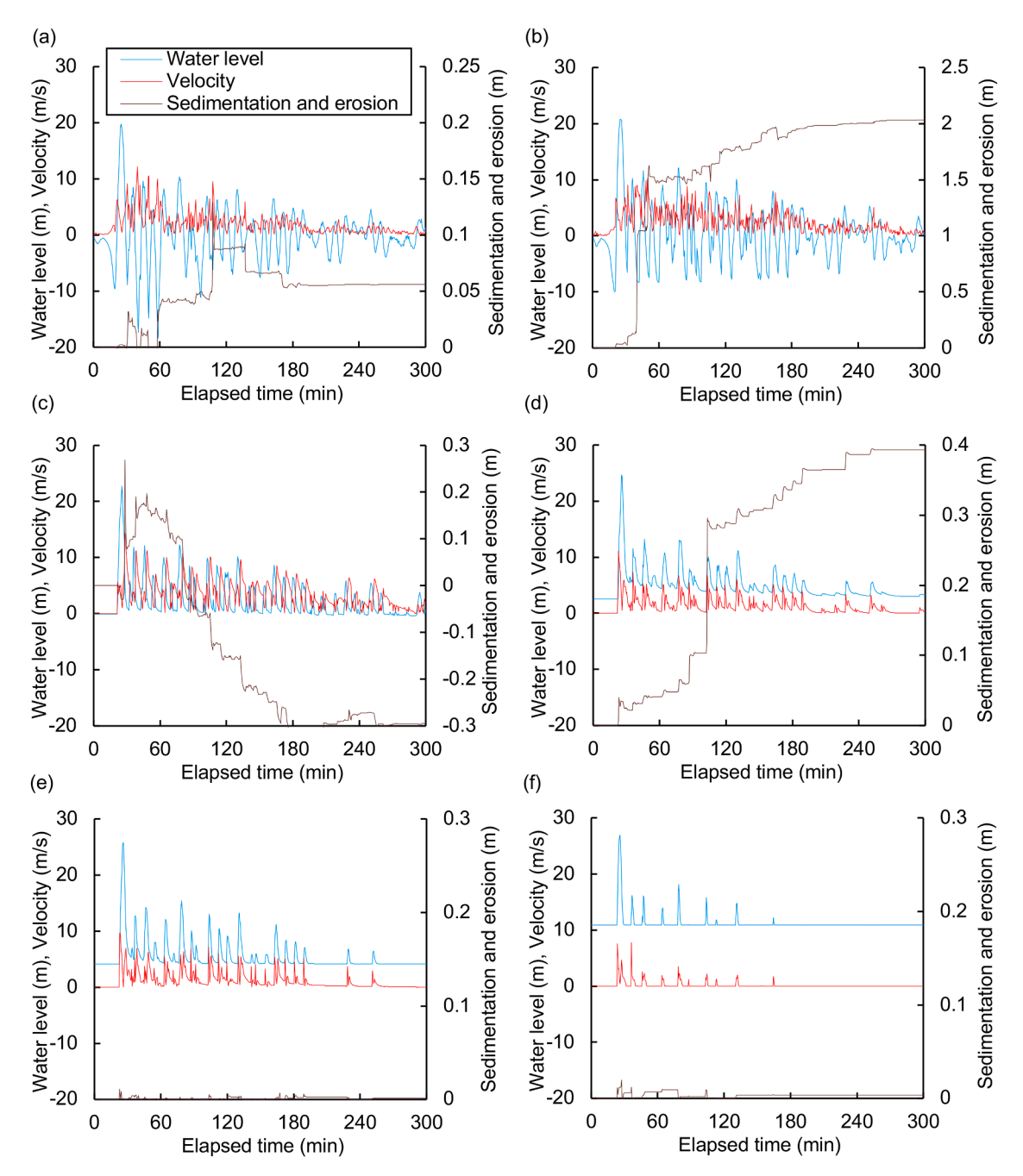


Fig. 10. The calculated water levels, topography, vertical velocity due to groundwater flow, and sediment transport rate at (a), (b) 22 min (when the tsunami reached the shoreline), (c), (d) 24 min, (e), (f) 26 min (when the tsunami reached its maximum inland inundation extent), and (g), (h) 35 min (during backwash).

by a tsunami by extending a one-dimensional XBeach-G model to account for the process in two dimensions.

The extended XBeach-G model can reproduce the observed waveform and time series of propagated solitary waves during laboratory experiments. This study then simulated gravel transportation by the 2011 Tohoku-oki tsunami at Koyadori, Japan. The extended XBeach-G model was found to accurately reproduce the observed distribution of onshore gravel deposits. Furthermore, infiltration and exfiltration have

been shown to influence the geomorphological changes caused by tsunamis on gravel coasts. In the simulation of this study, the inundation depth over land by the tsunami increased due to the exfiltration of groundwater, which affected the onshore deposition of gravel in the tsunami deposits. A calculation of groundwater flow has not been incorporated into tsunami modelling so far, but the results indicate that accounting for groundwater flow is important for both modelling tsunami inundation at gravel beaches and assessing gravel sediment



**Fig. 11.** The time series of calculated velocities, water depths, and thicknesses of the gravel deposits at (a) Obs 1 (735 m seaward from the shoreline, water depth is 20 m), (b) Obs 2 (215 m seaward from the shoreline, water depth is 10 m), (c) Obs 3 (the shoreline), (d) Obs 4 (215 m inland from the shoreline), (e) Obs 5 (405 m inland from the shoreline), (f) Obs 6 (635 m inland from the shoreline), The location of the observation points is shown in Fig. 4.

transport by a tsunami. However, choosing appropriate values for the sediment friction factor and multiplier in the equation for gravel transport is more important for reproducing the deposition of gravel sediments by a tsunami, as these parameters are more sensitive than the parameter of groundwater flow. When the parameter is set as  $f_s$  is 0.005,  $K_{lam}$  is 100 mms<sup>-1</sup>, and C is 13.6, the observed sediment volume over land was mostly reproduced.

The extended XBeach-G can potentially be used to investigate the gravel sediment transport process by a tsunami or reconstruct the size of paleotsunamis from gravel layers, while further validation of the extended XBeach-G model is recommended for this purpose.

# Data availability

The input file for the numerical modelling in this study was stored at <a href="https://data.mendeley.com/datasets/jd9m9w4hdn/1">https://data.mendeley.com/datasets/jd9m9w4hdn/1</a>. The code of the numerical simulation model developed in this study is available upon request.

#### **Funding**

This work was supported by Japan Society for the Promotion of Science under Grant No 21H00631, 21H04379, and 22K14455, the National Research Foundation, Singapore, and the National Environment Agency, Singapore under Grant No USS-IF-2020–2, and Singapore Ministry of Education Academic Research under Grant No MOE2019-

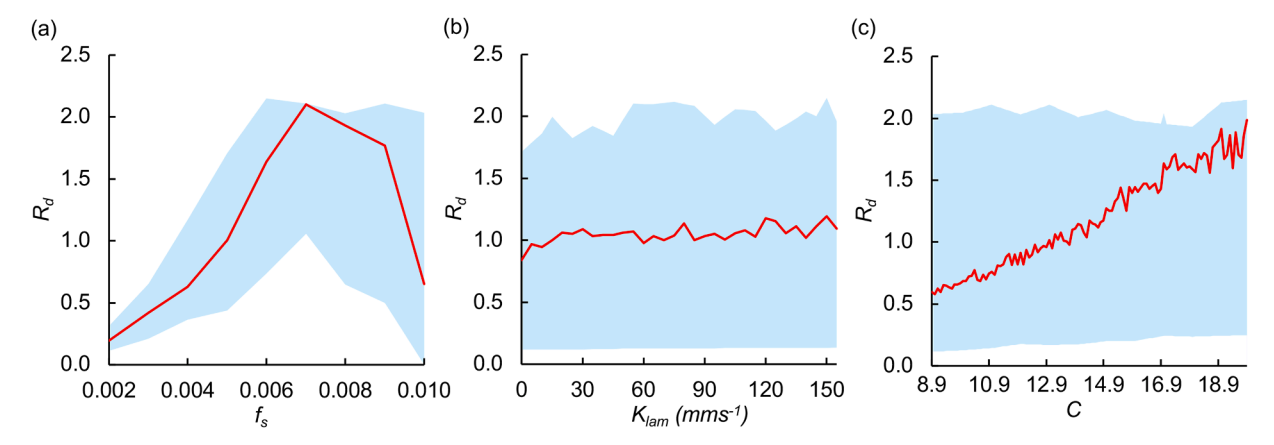


**Fig. 12.** The results of the sensitivity analysis. The relationship of  $R_d$  (Ratio of deposition volume to the observation result) and (a)  $f_s$  (Sediment friction factor), (b)  $K_{lam}$  (hydraulic conductivity), and (c) C (Multiplier in the equation for gravel transport). The red line is the value of  $R_d$  when the reference parameters ( $f_s = 0.005$ ,  $K_{lam} = 100 \text{ mms}^{-1}$ , C = 13.6) was used but the value of (a)  $f_s$ , (b)  $K_{lam}$ , and (c) C were changed. The blue area is the range of calculated  $R_d$ .

T3-1-004.

#### Ethical approval

Not applicable.

# CRediT authorship contribution statement

Masashi Watanabe: Writing – review & editing, Writing – original draft, Visualization, Validation, Software, Project administration, Methodology, Investigation, Funding acquisition, Formal analysis, Data curation, Conceptualization. Gerd Masselink: Writing – review & editing, Visualization, Validation, Supervision, Methodology, Investigation. Daisuke Ishimura: Writing – review & editing, Validation, Methodology, Funding acquisition, Data curation, Conceptualization. Masaki Yamada: Writing – review & editing, Methodology, Data curation. Adam D. Switzer: Writing – review & editing, Supervision, Funding acquisition, Conceptualization.

### Declaration of competing interest

The authors declare the following financial interests/personal relationships which may be considered as potential competing interests: Masashi Watanabe and Daisuke Ishimura reports financial support was provided by Japan Society for the Promotion of Science. Adam D. Switzer reports financial supports were provided by the National Research Foundation, Singapore, the National Environment Agency, Singapore, and Singapore Ministry of Education Academic Research.

# Acknowledgements

We thank Dr. Robert T. McCall for providing valuable suggestions and comments and helping with the description of the model formulations. The Miyako Agriculture and Forestry Promotion Centre of the Coastal Regional Development Bureau provided boring information. This research was financially supported by JSPS KAKENHI Grant Numbers 21H00631, 21H04379 and 22K14455. This Research/Project is supported by the National Research Foundation, Singapore, and the National Environment Agency, Singapore, under the National Sea Level Programme Funding Initiative (Award No USS-IF-2020–2) and Singapore Ministry of Education Academic Research Fund MOE2019-T3–1–004. The EOS contribution number is 586. We greatly appreciate Dr Pavel Adamek of Nanyang Technological University for proofreading the English text.

#### References

Abe, T., Goto, K., Sugawara, D., 2012. Relationship between the maximum extent of tsunami sand and the inundation limit of the 2011 Tohoku-oki tsunami on the Sendai Plain, Japan. Sediment. Geol. 282, 142–150.

Abe, T., Goto, K., Sugawara, D., 2020. Spatial distribution and sources of tsunami deposits in a narrow valley setting—Insight from 2011 Tohoku-oki tsunami deposits in northeastern Japan. Prog. Earth. Planet. Sci. 7 (1), 7.

Apotsos, A., Gelfenbaum, G., Jaffe, B., Watt, S., Peck, B., Buckley, M., Stevens, A., 2011a.

Tsunami inundation and sediment transport in a sediment-limited embayment on American Samoa. Earth-Sci. Rev. 107, 1–11.

Apotsos, A., Gelfenbaum, G., Jaffe, B., 2011b. Process-based modelling of tsunami inundation and sediment transport. J. Geophys. Res. -. Earth. Surf. 116, F01006.
 Austin, M.J., Masselink, G., 2006. Swash–groundwater interaction on a steep gravel beach. Cont. Shelf. Res 26 (20), 2503–2519.

Austin, M.J., Masselink, G., McCall, R.T., Poate, T.G., 2013. Groundwater dynamics in coastal gravel barriers backed by freshwater lagoons and the potential for saline intrusion: two cases from the UK. J. Mar. Syst 123–124 (0), 19–32.

Bellos, C., Hrissanthou, V., 2003. Numerical simulation of morphological changes in rivers and reservoirs. Comput. Math. Appl. 45, 453–467.

Darcy, H., 1856. Les Fontaines Publiques De La Ville De Dijon. Dalmont, Paris, France. French.

De Beer, A.F., McCall, R.T., Long, J.W., Tissier, M.F.S., Reniers, A.J.H.M., 2021.
Simulating wave runup on an intermediate-reflective beach using a wave-resolving and a wave-averaged version of XBeach. Coast. Eng. 163, 103788.

De Ridder, M.P., Smit, P.B., van Dongeren, A.R., McCall, R.T., Nederhoff, K., Reniers, A. J., 2021. Efficient two-layer non-hydrostatic wave model with accurate dispersive behaviour. Coast. Eng. 164, 103808.

Deltares, 2020. User Manual Delft3D-FLOW. 3.15.66766.

Deltares, 2015. XBeach Documentation. <. https://xbeach.readthedocs.io. >.
Dimakopoulos, A.S., Guercio, A., Cuomo, G., 2014. Advanced numerical modelling of tsunami wave propagation, transformation and run-up. Proc. Inst. Civ. Eng. -. Eng. Comput. Mechan 167 (3), 139–151.

Fritz, H.M., Phillips, D.A., Okayasu, A., Shimozono, T., Liu, H., Mohammed, F., Skanavis, V., Synolakis, C.E., Takahashi, T., 2012. The 2011 Japan tsunami current velocity measurements from survivor videos at Kesennuma Bay using LIDAR. Geophys. Res. Lett 39, L00G23.

Gelfenbaum, G., Vatvani, D., Jaffe, B., Dekker, F., 2007. Tsunami inundation and sediment transport in the vicinity of coastal mangrove forest. Coast. Sediments 07, 1117–1128

Haraguchi, T., Iwamatsu, A., 2011. Detailed Maps of the Impacts of the 2011 Japan tsunami: Vol. 1: Aomori, Iwate and Miyagi prefectures. Kokon-Shoin Publishers Ltd, Tokyo.

Hayashi, S., Koshimura, S., 2013. The 2011 Tohoku Tsunami flow velocity estimation by the aerial video analysis and numerical modeling. J. Disaster. Res. 8 (4), 561–572.

Horn, D., Li, L., 2006. Measurement and modelling of gravel beach groundwater response to wave run-up: effects on beach profile changes. J. Coast. Res 22 (5), 1241–1249

Hsu, S., Hsu, S.M., 2022. Morphological evolution mechanism of Gravel-bed braided river by numerical simulation on Da-jia River. J. Hydrol 613 (A), 128222.

Huang, Y., Zhu, C., 2015. Numerical analysis of tsunami-structure interaction using a modified MPS method. Nat. Hazards 75, 2847–2862.

Imamura, F., Goto, K., Ohkubo, S., 2008. A numerical model for the transport of a boulder by tsunami. J. Geophys. Res. 113, C01008.

Imamura, F., Koshimura, S., Oie, T., Mabuchi, Y., Murashima, Y., 2012. Tsunami Simulation For the 2011 Off the Pacific coast of Tohoku earthquake (Tohoku University model Version 1.2). Available at http://www.tsunami.civil.tohoku.ac. jp/hokusai3/J/events/tohoku\_2011/model/dcrc\_ver1.2.pdf. Accessed date: 26 October 2022.

- Inoue, T., Goto, K., Nishimura, Y., Watanabe, M., Iijima, Y., Sugawara, D., 2017.
  Paleotsunami history along the Northern Japan Trench: evidence from Noda Village, northern Sanriku coast, Japan. Prog. Earth. Planet. Sci 4, 42. https://doi.org/10.1186/s40645-017-0158-1.
- Ishimura, D., Miyauchi, T., 2015. Historical and paleo-tsunami deposits during the last 4000 years and their correlations with historical tsunami events in Koya-dori on the Sanriku Coast, northeastern Japan. Prog. Earth. Planet. Sci 2. https://doi.org/ 10.1186/s40645-015-0047-4.
- Ishimura, D., Ichihara, T., Sakata, T., Ohata, M., Takada, Y., 2015. Continuity of tsunami deposits and their correlations based on close interval Handy Geoslicer survey: case study of Koyadori, Yamada Town, Iwate Prefecture, northeast Japan. Act. Fault. Res 43, 53–60. Jananese.
- Ishimura, D., Yamada, K., 2019. Palaeo-tsunami inundation distances deduced from roundness of gravel particles in tsunami deposits. Sci. Rep 9, 10251.
- Ishimura, D., Yamada, K., 2021. Integrated lateral correlation of tsunami deposits during the last 6000 years using multiple indicators at Koyadori, Sanriku Coast northeast Japan. Quat. Sci. Rev 256, 106834.
- Jamal, M.H., Simmonds, D.J., Magar, V., 2014. Modelling gravel beach dynamics with XBeach. Coast. Eng 89, 20–29.
- Japan Hydrographic Association, 2001. Digital Bathymetric Chart M7005 Ver.2.3 Offshore Sanriku Coast.
- Kotani, M., Imamura, F., Shuto, N., 1998. Tsunami run-up simulation and damage estimation by using geographical information system. Proc. Coast. Eng 45, 356–360. Japanese.
- Li, L., Qiu, Q., Huang, Z., 2012. Numerical modeling of the morphological change in Lhok Nga, west Banda Aceh, during the 2004 Indian Ocean tsunami: understanding tsunami deposits using a forward modeling method. Nat. Hazards 64, 1549–1574.
- Masselink, G., McCall, R.T., Poate, T.G., van Geer, P., 2014. Modelling storm response on gravel beaches using XBeach-G. Proc. Inst. Civ. Eng. Marit. Eng 167 (MA4), 173–191.
- Masuda, H., Sugawara, D., Abe, T., Goto, K., 2022. To what extent tsunami source information can be extracted from tsunami deposits? Implications from the 2011 Tohoku-oki tsunami deposits and sediment transport simulations. Prog. Earth. Planet. Sci. 9 (1), 1–20.
- McCall, R., Masselink, G., Poate, T., Roelvink, J., Almeida, L., Davidson, M., Russell, P., 2014. Modelling storm hydrodynamics on gravel beaches with XBeach-G. Coast. Eng 91, 231–250.
- McCall, R.T., 2015. Doctoral dissertation. Plymouth University.
- McCall, R.T., Masselink, G., Poate, T.G., Roelvink, J.A., Almeida, L.P., 2015. Modelling the morphodynamics of gravel beaches during storms with XBeach-G. Coast. Eng 103, 52-66.
- Madsen, P., Fuhruman, D., SchaXer, H., 2008. On the solitary wave paradigm for tsunamis. J. Geophys. Res.:. Oceans 113. C12012.
- Meyer-Peter, E., Müller, R., 1948. Formulas for bed-load transport. In: Proc. 2nd Meet. Int. Assoc. Hydraul. Res..
- Moore, A., 2000. Landward fining in onshore gravel as evidence for a late pleistocene tsunami on Molokai, Hawaii. Geology 28 (3), 247–250.
- Mori, N., Takahashi, T., Yasuda, T., Yanagisawa, H., 2011. Survey of 2011 Tohoku earthquake tsunami inundation and run-up. Geophys. Res. Lett 38, L00G14.
- Murakami, S., 1993. Comparison of various turbulence models applied to a bluff body. J. Wind. Eng. Ind. Aerodyn 46 and 47, 21–36.
- Nielsen, P., 2002. Shear stress and sediment transport calculations for swash zone modelling. Coast. Eng 45 (1), 53–60.
- Nichol, S., Lian, O.B., Carter, C.H., 2003. Sheet-gravel evidence for a late holocene tsunami run-up on beach dunes, Great Barrier Island, New Zealand. Sediment. Geol 155 (1–2) 129–145.
- NOAA, 2025. Benchmark Methods for Tsunami Model Validation and Verification.

  Available at https://nctr.pmel.noaa.gov/benchmark/. Accessed date: 16 July 2025.
- Okada, Y., 1985. Surface deformation due to shear and tensile faults in a half-space. Bull. Seismol. Soc. Am. 75, 1135–1154.
- Poate, T., Masselink, G., Davidson, M., McCall, R., Russell, P., Turner, I., 2013. High frequency in-situ field measurements of morphological response on a fine gravel beach during energetic wave conditions. Mar. Geol 342, 1–13.
- Poate, T., Masselink, G., McCall, R., Russell, P., Davidson, M., 2014. Storm-driven cusp behaviour on a high energy gravel beach. In: Journal of Coastal Research Special Issue 70, Proceedings 13th International Coastal Symposium. Durban, South Africa, pp. 645–650.
- Poate, T., McCall, R., Masselink, G., 2016. A new parameterisation for runup on gravel beaches. Coast. Eng. 117, 176–190.
- Quataert, E., Storlazzi, C., van Dongeren, A., McCall, R., 2020. The importance of explicitly modelling sea-swell waves for runup on reef-lined coasts. Coast. Eng. 160, 103704.
- Roelvink, J.A., Reniers, A., van Dongeren, A.R., van Thiel de Vries, J.S.M., McCall, R., Lescinski, J., 2009. Modeling storm impacts on beaches, dunes and barrier islands. Coast. Eng. 56, 1133–1152.
- Shinozaki, T., Yamaguchi, N., Sekiguchi, T., 2020. Flume experiments test grain-size distribution of onshore tsunami deposits. Sediment. Geol. 407, 105750.
- Simpson, D.P., 2005. Gravel beaches. In: Schwartz, M.L. (Ed.), Encyclopedia of Coastal Science. Encyclopedia of Earth Science Series. Springer, Dordrecht. https://doi.org/ 10.1007/1-4020-3880-1 159.

- Simpson, G., Castelltort, S., 2006. Coupled model of surface water flow, sediment transport and morphological evolution. Comput. Geosci 32, 1600–1614.
- Smagorinsky, J., 1963. General circulation experiments with the primitive equations I. The basic experiment. Mon. Weather. Rev. 91, 99–164.
- Smit, P., Stelling, G., Roelvink, J., Van Thiel de Vries, J., McCall, R., Van Dongeren, A., Zwinkels, C., Jacobs, R., 2010. XBeach: Non-hydrostatic model: Validation, Verification And Model Description. Tech. rep. Delft University of Technology.
- Soulsby, R.L., Whitehouse, R.J.S.W., 1997. Threshold of sediment motion in coastal environments. In: Pacific Coasts and Ports' 97 Conference. Christchurch, New Zealand. Univ. of Canterbury.
- Sugawara, D., Takahashi, T., Imamura, F., 2014. Sediment transport due to the 2011 Tohoku-oki tsunami at Sendai: results from numerical modeling. Mar. Geol 358, 18–37
- Sugawara, D., Yu, N.T., Yen, J.Y., 2019. Estimating a tsunami source by sediment transport modeling: a primary attempt on a historical/1867 normal-faulting tsunami in Northern Taiwan. J. Geophys. Res. Earth. Surf 124 (7), 1675–1700.
- Sugino, H., Wu, C., Korenaga, M., Nemoto, M., Iwabuchi, Y., Ebisawa, K., 2013. Analysis and verification of the 2011 Tohoku Earthquake Tsunami at nuclear power plant sites. J. Jpn. Assoc. Earthq. Eng. 13, 2–21.
- Synolakis, C.E., 1987. The run-up of solitary waves. J. Fluid. Mech 185, 523-545.
- Szczuciński, W., Rachlewicz, G., Chaimanee, N., Saisuttichai, D., Tepsuwan, T., Lorenc, S., 2012. 26 December 2004 tsunami deposits left in areas of various tsunami runup in coastal zone of Thailand. Earth. Planets. Space 64, 843–858.
- Takahashi, T., Imamura, F., Shuto, N., 1992. Development of a tsunami calculation method with sediment transport. Proc. Coast. Eng. 39, 231–235. Japanese.
- Takeda, H., Goto, K., Goff, J., Matsumoto, H., Sugawara, D., 2018. Could tsunami risk be underestimated using core-based reconstructions? Lessons from ground penetrating radar. Earth. Surf. Process. Landf. 43 (4), 808–816.
- Tanaka, H., Yoshitake, Y., Shuto, N., 1989. Numerical simulation of bottom deposit classification in wave and flow coexisting field. Proc. Coast. Eng. 36, 264–268. Japanese.
- The Geospatial Information Authority of Japan, 2025a. The Geospatial Information map (Electronic National Land Web). Available at https://maps.gsi.go.jp/#5/36.1046 11/140.084556/&base=std&ls=std&disp=1&vs=c1g1j0h0k0l0u0t0z0r0s0m0f1. Accessed date: 16 July 2025.
- The Geospatial Information Authority of Japan, 2025b. The Information For the Fundamental Map is in the Download service. Available at https://fgd.gsi.go.jp/download/menu.php. Accessed date: 16 July 2025.
- Turner, I.L., Masselink, G., 2012. Coastal gravel barrier hydrology observations from a prototype-scale laboratory experiment (BARDEX). Coast, Eng 63, 13–22.
- Van, C.P., Chua, V., 2020. Numerical simulation of hydrodynamic characteristics and bedload transport in cross sections of two gravel-bed rivers based on onedimensional lateral distribution method. Int. J. Sediment. Res. 35 (2), 203–216.
- Watanabe, M., Goto, K., Bricker, J.D., Imamura, F., 2018. Are inundation limit and maximum extent of sand useful for differentiating tsunamis and storms? An example from sediment transport simulations on the Sendai Plain, Japan. Sediment,. Geol 364, 204–216.
- Watanabe, M., Goto, K., Roeber, V., Imamura, F., 2021. Identification of coastal sand deposits from tsunamis and storm waves based on numerical computations. J. Geophys. Res.:. Earth. Surf. 126, e2021JF006092.
- Watanabe, M., Arikawa, T., Kihara, N., Tsurudome, C., Hosaka, K., Kimura, T., Hashimoto, T., Ishihara, F., Shikata, T., Morikawa, D.S., Makino, T., Asai, M., Chida, Y., Ohnishi, Y., Marras, S., Mukherjee, A., Cajas, J.C., Houzeaux, G., Paolo, B. D., Lara, J.L., Barajas, G., Losada, Í.L., Hasebe, M., Shigihara, Y., Asai, T., Ikeya, T., Inoue, S., Matsutomi, H., Nakano, Y., Okuda, Y., Okuno, S., Ooie, T., Shoji, G., Tateno, T., 2022. Validation of tsunami numerical simulation models for an idealized coastal industrial site. Coast. Eng. J. 64 (2), 302–343.
- Watanabe, M., Arikawa, T., 2023. Elucidation of wave pressure acting on a wave-cut notch beneath a coastal cliff based on laboratory experiments and numerical modeling. Ocean. Eng. 270, 113656.
- Watanabe, M., Bricker, J.D., Goto, K., Imamura, F., 2017. Factors responsible for the limited inland extent of sand deposits on Leyte Island during 2013 Typhoon Haiyan. J. Geophys. Res. Oceans 122 (4), 2795–2812.
- Watanabe, M., Goto, K., Abe, T., 2023a. Can mud deposits indicate inundation extent of paleotsunamis? Insights from sand/mud sediments transport simulation. J. Geophys. Res.:. Earth. Surf. 128, e2023JF007137.
- Watanabe, M., Yoshii, T., Roeber, V., Goto, K., Imamura, F., 2023b. Derivation, validation, and numerical implementation of a two-dimensional boulder transport formulation by coastal waves. J. Earthq. Tsunami 17, 2250018.
- Williams, J., Buscombe, D., Masselink, G., Turner, I., Swinkels, C., 2012. Barrier dynamics experiment (BARDEX): aims, design and procedures. Coast,. Eng 63 (0), 2, 12
- Xiao, H., Young, Y.L., Prevost, J.H., 2010. Hydro- and morpho-dynamic modelling of breaking solitary waves over a fine sand beach. Part II: numerical simulation. Mar, Geol 269 (3–4), 119–131.
- Yamada, M., Fujino, S., Goto, K., 2014. Deposition of sediments of diverse sizes by the 2011 Tohoku-oki tsunami at Miyako City, Japan. Mar,. Geol 358, 67–78.
- Yoshida, T., Ohsawa, A., Katada, M., 1984. Geological Map of Japan 1:200,000. Geological Survey of Japan, Tsukuba, Morioka.